

## DEBRIS DISKS IN NGC 2547

N. GORLOVA<sup>1,2</sup>, Z. BALOG<sup>2</sup>, G. H. RIEKE<sup>2</sup>, J. MUZEROLLE<sup>2</sup>, K. Y. L. SU<sup>2</sup>, V. D. IVANOV<sup>3</sup>, E. T. YOUNG<sup>2</sup>

<sup>1</sup>Department of Astronomy, University of Florida, Gainesville, FL 32611-2055, *ngorlova@astro.ufl.edu*

<sup>2</sup>Steward Observatory, University of Arizona, 933 North Cherry Avenue, Tucson, AZ 85721-0065 and

<sup>3</sup>European Southern Observatory, Ave. Alonso de Cordova 3107, Casilla 19, Santiago 19001, Chile

*to appear in ApJ*

### ABSTRACT

We have surveyed the 30 Myr-old cluster NGC 2547 for planetary debris disks using *Spitzer*. At 4.5–8  $\mu\text{m}$  we are sensitive to the photospheric level down to mid-M stars ( $0.2 M_{\odot}$ ) and at 24  $\mu\text{m}$  to early-G stars ( $1.2 M_{\odot}$ ). We find only two to four stars with excesses at 8  $\mu\text{m}$  out of  $\sim 400$ –500 cluster members, resulting in an excess fraction  $\lesssim 1\%$  at this wavelength. By contrast, the excess fraction at 24  $\mu\text{m}$  is  $\sim 40\%$  (for B–F types). Out of four late-type stars with excesses at 8  $\mu\text{m}$  two marginal ones are consistent with asteroid-like debris disks. Among stars with strong 8  $\mu\text{m}$  excesses one is possibly from a transitional disk, while another one can be a result of a catastrophic collision. Our survey demonstrates that the inner 0.1–1 AU parts of disks around solar-type stars clear out very thoroughly by 30 Myrs of age. Comparing with the much slower decay of excesses at 24 and 70  $\mu\text{m}$ , disks clear from the inside out, of order 10 Myr for the inner zones probed at 8  $\mu\text{m}$  compared with a hundred or more Myr for those probed with the two longer wavelengths.

*Subject headings:* infrared: stars — circumstellar matter — planetary systems: formation — open clusters and associations

### 1. INTRODUCTION

The 5 to 50 Myr age range is critical for tracing the formation of terrestrial planets. At the beginning of this range, protoplanetary disks are ending their lives, the gas has mostly escaped the system, and the remaining material is in the form of solid bodies that do not yet approach planetary scale (Meyer et al. 2006; Hernández et al. 2005; Pascucci et al. 2006; Sicilia-Aguilar et al. 2007). By the end of the range, planetary embryos thousands of kilometers in size have formed in the inner few AU zone (Chambers 2001; Kenyon & Bromley 2006). They are capable of stirring up smaller bodies and creating collisional cascades, forming debris disks that might take a number of forms, such as a single ring (Kenyon & Bromley 2004a), or of numerous rings in the presence of giant planets that gravitationally scatter and trap dust into resonances (Moro-Martín & Malhotra 2002). The Earth-Moon system was created in a grand collision at this age (Kleine et al. 2002). These debris systems are warmed by the central stars and emit in the mid- and far-infrared. Therefore, by studying the infrared excess emission of stars over this range of ages, we can characterize some features of the early evolution of terrestrial planets.

NGC 2547 is an excellent target to examine the late stages of this critical period. It is a rich open cluster in the Southern Hemisphere at a distance of 400–450 pc (Clariá 1982; Naylor et al. 2002). Clariá (1982) was first to carry out an extensive photoelectric survey (in the *UBV* bands) and determine its main properties. He identified 70 members up to  $V = 13.4^m$  (B3 to  $\sim$ K0) and estimated the age to be between 30 and 80 Myr from the brightest members at the Main Sequence (MS) turn off. Despite lying only  $8^{\circ}$  from the Galactic plane, the cluster was found to have only a small amount of reddening,  $E(B-V) = 0.06 \pm 0.02$ . Jeffries & Tolley (1998) and Naylor et al. (2002) extended the cluster sequence

further down to  $V = 20^m$  (mid-Ms or  $\sim 0.2 M_{\odot}$ , according to the models of Siess et al. (2000)), by carrying out a *BVI* survey within  $15'$  from the cluster center and identifying counterparts to *ROSAT* sources. Recently, Jeffries et al. (2004) performed an *RIZ* survey identifying members in the substellar domain (down to 0.05  $M_{\odot}$ ). Jeffries & Tolley (1998) inferred an age of 10–20 Myr from isochronal fitting to the low mass pre-MS population, at odds with the estimate of  $\sim 50$  Myr from the cluster turn-off (though the latter is defined by only one or two stars). The first measurements of lithium depletion in the K–M members again favored 50 Myr, casting doubt on the validity of the pre-MS evolutionary models (Jeffries et al. 2003; Oliveira et al. 2003). The age discrepancy was finally reconciled at  $30 \pm 5$  Myr based on more precise observations of X-rays with *XMM-Newton* (Jeffries et al. 2006) and of the Li depletion boundary with the VLT (Jeffries & Oliveira 2005). The most recent *UBVRI* study of Lyra et al. (2006) confirms a 30–40 Myr age range after fitting four independent contraction tracks; the distance and reddening from this study are on the low side of the previous range of estimates (390 pc and  $E(B-V) = 0.03$ ).

By comparing the disk population in NGC 2547 with clusters and field stars of different ages we can verify whether indeed this age corresponds to a high level of planetesimal activity, and whether the time-scale for inner planet formation differs among stars of various masses. The *Spitzer* survey of Young et al. (2004) demonstrated the lack of dust near the sublimation temperature for the bulk of members down to mid-K, while  $\sim 200$  K dust was found for a quarter of the early-type members. An ambiguity remained for late K–M stars however, where mid-IR excesses were marginally detected in a dozen stars. The uncertainty was partly due to measurement errors, but also due to low number statistics of known members for the empirical determi-

nation of the photospheric locus in the *Spitzer* bands.

The present study is a re-analysis of the *Spitzer* data for NGC 2547 first presented in Young et al. (2004). That study was performed early in the *Spitzer* mission; we can now use improved image processing techniques and flux calibrations, resulting in more precise photometry. Secondly, to identify debris disks we apply improved color-selection criteria developed in the successive studies of other clusters, within the framework of the MIPS open cluster survey (Gorlova et al. 2004, 2006; Siegler et al. 2006). Thirdly, we use a new extended membership list, allowing an improvement in the statistical significance of the results. We therefore can probe disks around the lower mass stars and over the full area covered by *Spitzer*. Finally, we report a multi-slit medium-resolution spectroscopic survey of a subsample of photometric members. We improve the spectroscopic membership list for F-M stars and confirm chromospheric emission in K and M members, a result that was somewhat ambiguous in previous studies.

## 2. OBSERVATIONS AND DATA REDUCTION

### 2.1. *Spitzer* Photometry

*Spitzer* observed a  $\sim 1^\circ$ -wide area centered on NGC 2547 with the IRAC and MIPS instruments at 3.6, 4.5, 5.8, 8.0, and 24  $\mu\text{m}$  central wavelengths. Observations of NGC 2547 with IRAC were obtained on Dec 19, 2003. The high dynamic range mode survey with integration times of 0.4 s and 10.4 s covers about half a square degree centered on RA=08:10:13 and DEC=−49:13:25. The observation was repeated twice in each position giving a total of 20.8 s integration time. The BCD frames from the SSC pipeline 13.2 were processed and mosaiced using a custom IDL program provided by the IRAC team. We then performed photometry for a new member list (§3). Source finding and aperture photometry for IRAC were carried out using PhotVis version 1.10 which is an IDL-GUI based photometry visualization tool (Gutermuth et al. 2004). The radii of the source aperture, and the inner and outer sky annuli were at 2.4, 2.4 and 7.2 arc-second respectively. We converted the MJy/sr units to DN/s using conversion factors 0.1088, 0.1388, 0.5952, and 0.2021 for channels 1, 2, 3, and 4 respectively. Then we calculated the standard IRAC magnitudes using  $-2.5 \cdot \log(\text{flux}_{\text{DN/s}}) + \text{zp}$  where  $\text{zp}$  is 21.9929, 21.2583, 19.0747 and 19.4372 for channels 1–4 respectively. The zero point term  $\text{zp}$  includes: 1) the zero point of the flux to magnitude transformation based on the large aperture measurements of a standard star (19.66, 18.94, 16.88, 17.39 mag for channels 1–4); 2) the aperture corrections to account for the difference between the aperture sizes used for the standard star and for NGC 2547 photometry (−0.21, −0.23, −0.35 and −0.50 mag for channels 1–4); 3) 2.54 mag correction for exposure time in the mosaic. Originally we accepted all sources with photometric error less than 0.2 mag as good detections, then we examined the detected sources visually to clean the sample of spurious detections and non-stellar objects. However, because the IRAC images were obtained with only two dithers, this procedure is limited at removing the effects of the cosmic rays. This issue is discussed further in §4.1. We compared our photometry with the photometry of Young et al. (2004) and found

that the two datasets agree within the errors. The IRAC counterparts of the known members of NGC 2547 were found using a 2" matching radius.

The Multi-band Imaging Photometer for Spitzer (MIPS) observed NGC 2547 at 24  $\mu\text{m}$  on Jan 28, 2004 (Young et al. 2004). We used the image of Young et al. (2004) but re-did the photometry. At 24  $\mu\text{m}$  we performed PSF-fitting photometry; this approach is preferred (compared to the aperture photometry we used with IRAC data) because of the good PSF sampling; it also helps suppress the effects of the complex background at this wavelength. The procedure was identical to that Gorlova et al. (2006) initially applied to the Pleiades. Briefly, we first applied the IRAF package `daophot`, task `phot` to obtain aperture photometry for the cluster members based on 2MASS coordinates. We used these results as input into task `allstar` with the template PSF constructed from 19 isolated stars in our image with a range of brightness. The calibration of the PSF-fitting photometry is based on a comparison of it with the aperture photometry of these isolated, well-measured stars. To put instrumental magnitudes produced by `allstar` into the “Vega system”, we used the following conversion factors: the aperture correction for an aperture radius of 3.5 px (1 pixel= 1.247") and sky annulus from 5 to 10.5 pixels is 0.86 mag; 1 DN/s/px= 1.63742E-06 Jy/px; [24] = 0<sup>m</sup> is equivalent to 7.14 Jy. The `allstar` re-centered coordinates deviate by no more than 2" from 2MASS coordinates, except for a few of the faintest members and bright extended objects.

Our *Spitzer* photometry for optical candidate members is given in Tables 1 and 2. Out of 860 objects we detect 606, 638, 589, 582, and 84 at maximum magnitudes 15.5, 15.7, 15.4, 15.0, and 11.7 in IRAC channels 1–4 and at MIPS 24  $\mu\text{m}$  respectively. We achieve 3–5 times more detections and go 1–2 mag deeper than Young et al. (2004). Figure 1 shows the *Spitzer* view of NGC 2547 composed of the 4.5, 8 and 24  $\mu\text{m}$  maps. Fig. 2 shows the 8  $\mu\text{m}$  image onto which we have overplotted the optical members, those detected at 4.5, 8, and 24  $\mu\text{m}$  respectively, and the subsample we observed spectroscopically. The IRAC images have a good match in depth and coverage to the optical surveys (except for a 0.2° NE offset of the 3.5 and 5.8  $\mu\text{m}$  channels from the cluster center). The MIPS coverage is only slightly smaller in the NS direction, but confusion with background sources and interstellar (ISM) nebulosity limits its sensitivity to intermediate mass members in the center of the cluster.

### 2.2. Multi-slit Spectroscopy

To evaluate the level of contamination of our sample of photometrically selected members, as well as to investigate the properties of excess sources, we have obtained medium-resolution spectra in the red for a number of candidate members, covering a wide range of spectral types from B to mid-M. These sources are marked by open circles in the color-color plots in this paper.

The observations were performed in two runs in 2005 with the multi-object spectrograph IMACS on the 6.5m Baade telescope (Magellan-1) at Las Campanas, Chile. The atmospheric conditions were excellent with seeing typically around 0.6". We observed 3 fields with 5 masks. Two 15'  $\times$  15' fields were centered on the cluster center and one was adjacent to the North-West (Table 3, Fig.

2). For the central fields we created separate masks for bright stars ( $V = 8-13^m$ ) and faint stars ( $V = 13-20^m$ ) to avoid bleeding from the bright stars in long exposures. The faint masks contained 20–30 slits each. About a quarter of the spectra were rejected in the final analysis due to overlap with other spectra, closeness to chip edges, or underexposure.

We observed with the f/4 camera,  $2 \times 2$  binning (for higher S/N),  $6'' \times 0.7''$  slits and the 1200 lines/mm grating, at the maximum available angle of  $32^\circ.8$  in 1st order. The spectra were dispersed across 4 chips resulting in 3 gaps  $\sim 100 \text{ \AA}$ -wide. The aim was to target the region around the Ca II IR triplet at  $8500-8700 \text{ \AA}$  at the maximum resolution. With a plate scale of  $0.22''/\text{binned pixel}$ , this resulted in resolution of  $1 \text{ \AA}$  (for  $0.6''$  seeing), or  $R = 8,200$  ( $36 \text{ km/s}$ ) at the central wavelength of  $8350 \text{ \AA}$ . When reducing the data however we discovered that the filter we used transmitted also in the 2nd order, contaminating the targeted red region with  $3600-4750 \text{ \AA}$  flux. This affects mostly F-K stars that have strong metallic lines in the blue. The effect is reduced at higher airmass. We alleviated the order overlap problem by carrying out a spectral analysis relative to several templates chosen from the sample itself (as discussed in §3.2), and also with reference to external digital libraries that cover both spectral regions.

We normally observed 3 science exposures, followed by quartz flat fields and He-Ne-Ar arcs. Bias frames were obtained every other night. The reduction was performed with the IMACS reduction package COSMOS, that performs alignment of the frames, summation with cosmic ray rejection, flat-fielding, wavelength calibration, sky subtraction and 2-dimensional spectrum extraction. Final extraction was performed with the IRAF task `apall`.

In total, we extracted spectra for 88 sources, 84 of which are in our member lists (Tables 1, 2). 2MASS 08093815-4918403 was resolved into 2 objects  $1''$  apart. With seeing of  $0.6''$ , the wings of the spectral PSFs overlap, so we carried out their extraction with reduced aperture size. The spectrum of the brighter source was given designation “a”, and of the fainter one “b”. One more object was resolved into a pair – 2MASS 08100398-4913027, but only the spectrum of the brighter star was extracted. The companion star is  $1.3''$  NE away, unresolved in 2MASS, and probably explains the non-stellar flag in Jeffries et al. (2004).

### 2.3. Near-Infrared Spectroscopy

For two solar-type members with strong *Spitzer* excesses, ID 8 & 9, we obtained K-band spectra targeting the CO band-head at  $2.3 \mu\text{m}$  to verify that these stars are not late-type interlopers. The spectra were obtained with SofI (Son of ISAAC; Moorwood et al. (1998)) at the ESO 3.6m NTT telescope on September 5, 2006. We used the medium resolution mode ( $R = 1300$ ) with a  $1''$  wide slit. The data were taken by nodding the target along the slit. For each target we obtained 4 images of 150 sec integration each.

The data reduction consisted of the usual steps: flat fielding, sky subtraction, and extraction of a one-dimensional spectrum from each frame. Then, we wavelength calibrated the spectra with images of Neon and Xenon lamps and combined the individual spectra into a

single spectrum. A B2.5 V star HIP 041781 and a G2 V HIP 43141 A were observed for telluric absorption correction. Both targets and standards were observed at a narrow airmass range of 1.4–1.5. Considering that the target stars were expected to be of G–K type, to preserve numerous weak atomic lines dominating their spectra, we preferred to divide out telluric absorption with a B rather than a G-type standard. The K-band spectrum of a main sequence B star is essentially featureless except for the  $\text{Br}\gamma$  line at  $2.166 \mu\text{m}$  (Hanson et al. 1996), which we removed by continuum interpolation before division. A G-type telluric standard was reduced in a similar way and served as a reference. The continuum shape of the final spectra was straightened with a low-order polynomial, to facilitate comparison of line strengths with spectroscopic standards from the literature (Sec. 6.2).

## 3. CLUSTER MEMBERSHIP

### 3.1. Photometric Sample

Young et al. (2004) used a sample of 184 stars from Naylor et al. (2002) with membership based on D’Antona & Mazzitelli (1997) (DM97) isochrones, of which 169 were detected at least in one IRAC band and 31 at  $24 \mu\text{m}$ . Rieke et al. (2005) report  $24 \mu\text{m}$  measurements for an additional 15 B-A members. Since then a deeper and wider survey has been carried out in the  $RIZ$  bands by Jeffries et al. (2004), that covers the central area within a  $30'$  radius from the cluster center, plus two fields  $60'$  away. Their  $RIZ$  sample consists of DM97 and Baraffe et al. (2002) (BCAH02) - selected objects (their Tables “A3” and “A2” respectively). In short, the selection process consisted of finding for each model a semi-empirical isochrone that best fits color-magnitude diagrams of X-ray sources in NGC 2547 and the brown dwarfs in the Pleiades, and identifying as members sources that lie 0.25 mag below and 0.9 mag above this isochrone, which accounts for the photometric errors and unresolved binaries respectively. For our survey we decided not to give preference to either of the evolutionary calculations and formed member sample by including all sources from both tables. The brightest stars were saturated in this survey, we therefore complemented it with the “enhanced catalog” from Littlefair et al. (2003) (“Table 1”) that is a combination of the Naylor et al. (2002)  $BVI$  “wide catalog” with the  $UBV$  catalog of Clariá (1982). The tables are available in electronic form at the Cluster Collaboration’s Photometric Catalog Page<sup>1</sup>.

A number of  $BV$ -selected candidate members do not have  $RIZ$  counterparts in Table “A2” or “A3” of Jeffries et al. (2004). They are however listed in their Table “A1”, which contains  $RIZ$  photometry for everything in the NGC 2547 field. After checking image quality flags for these sources, we retained in the main member list (Table 1) those that were omitted apparently because of the saturation in the  $RIZ$  bands. Those with non-stellar designation, flawed photometry due to bad pixels, closeness to the CCD edge, or problematic background, as well as fainter sources with good  $RIZ$  photometry but not placed into tables “A2” and “A3” anyway, were all moved into a separate table of less probable members (Table 2). After removal of  $\sim 4\%$  of sources without

<sup>1</sup> <http://www.astro.ex.ac.uk/people/timn/Catalogues/description.html>

2MASS counterpart within 2'', the total number of objects in the two tables is 860.

### 3.2. Spectroscopic Subsample

Because of the unfortunate overlap of the blue and red regions in our spectra, spectral classification is not trivial. To interpret the spectra we first plotted them along a sequence in  $V - K$  color, assuming that members would form a monotonic sequence of spectral line strengths from which excess members and interlopers might stand out. Fig. 3 shows representative spectra along this sequence, while Fig. 4 shows spectra of excess candidates (§4). The segments shown contain prominent features used in spectral classification.

We found variability in the strength of the blue spectrum that correlates with the airmass of observations. The February observations were obtained at a slightly larger airmass and the blue lines are weaker than in December. As a result, we can not accurately differentiate between late F to K classes based on the strength of such classical indicators as Ca II H & K, Balmer lines and the G-band. The IR Ca II triplet itself does not vary significantly between F–K types (Allen & Strom 1995; Carquillat et al. 1997), while the weaker Fe I and Ti I lines get mingled with metallic lines from the blue. On the other hand, we can confidently identify B–A types based on the presence of the Paschen series, and M types based on the K I and Na I strong lines in the red. Our analysis significantly expands the spectral characterization of the cluster population, which previously concentrated on the brightest B–A members and a few K–M stars for the Li studies.

To measure radial velocities, we split our spectroscopic sample into four groups that we designate “B–F”, “G”, “K” and “M”, with 13, 13, 40 and 23 objects respectively. The names of these radial velocity groups only roughly represent spectral types, due to variations in the visibility of the blue spectrum. Within each group we picked a template to use for cross correlation, requiring only for it to be of high S/N and contain no chip gaps or bad pixels in the main features of interest. These templates are 2MASS 08095066-4912493, 08095109-4859022, 08101944-4907444, and 08092437-4906282 respectively.

We measured the radial velocities of these templates using 3–6 lines of Ca II, Fe, Ti in the 8500–8700 Å interval with line identifications from Munari & Tomasella (1999). We obtained 27.4, 58.0, -20.6 and 21.1 km/s with an RMS uncertainty of few km/s. We then used the IRAF task `fxcor` to correlate the template spectra with the objects in each group in the same 8500–8700 Å region, and converted the relative wavelength shifts into heliocentric velocities. Robichon et al. (1999) reports the radial velocity for the cluster to be  $14.4 \pm 1.2$  km/s based on 5 stars, Clariá (1982) 15.4 km/s based on 10 stars, and Jeffries, Totten, & James (2000) 12.8 km/s  $\pm 0.9$  based on 20 stars. Since we did not observe radial velocity standards, to put our measurements on the absolute scale, we averaged our values in the M group (for which we achieved the highest accuracy) to obtain 21.7 km/s (with RMS =  $\pm 3.5$  for 22 stars) and then subtracted 8.9 km/s from all our values to put them on the same scale as in Jeffries, Totten, & James (2000).

The histograms of these adjusted radial velocities for

each radial velocity group and for all the groups together are plotted in Fig. 5, while the individual values are listed in Table 4. Two  $1\sigma$  error bars are shown in each panel of Fig. 5,  $\sigma_{abs} = 2\text{--}5$  km/s being the uncertainty of the standard star velocity determination, and  $\sigma_{rel} = 1\text{--}6$  km/s an average uncertainty of the relative velocity between the standard and a given star in the group. The first error gives the limit on the shift of the entire distribution along the x-axis, while the second error contributes to the width of the distribution.  $\sigma_{abs}$  is taken to be the RMS deviation from the mean when measuring velocity of the standard from several lines; it compares well with the uncertainty of the wavelength calibration of the arc lamp spectrum.  $\sigma_{rel}$  is calculated by `fxcor` based on the goodness of the match of the target and the shifted standard spectra; it only exceeds  $\sigma_{abs}$  in the BF group, due to the cross-correlation of the broader hydrogen lines. The larger  $\sigma_{abs}$  of the G standard is due to strong blending with the blue spectrum, which makes it difficult to identify clean lines for the radial velocity determination. A secondary peak at  $\sim 75$  km s $^{-1}$  in the K group is real and most certainly arises from contaminating background stars, as one might expect in this spectral range. Naylor et al. (2002) estimated that the contamination of the  $BVI$  sample by background stars is negligible, except in the  $14.0 < V < 15.5$  range where the cluster sequence crosses the “finger” of Galactic red giants and contamination is predicted to be as high as 40%. The combined histogram at the bottom panel does not include the 4 earliest type stars with the biggest  $v \sin i$  and discrepantly large radial velocities. It can be used to identify as potential non-members stars with radial velocity  $\gtrsim 50$  km/s. None of them appears among the 8  $\mu\text{m}$  excess objects, and only one has a possible 24  $\mu\text{m}$  excess (2MASS 08101474-4912320).

### 3.3. Proper Motions

As an additional constraint on membership, we analyzed proper motions for our photometric sample. The UCAC2 catalog and its bright stars supplement (Zacharias et al. 2003)<sup>2</sup> contain measurements for all NGC 2547 B–F stars and 86% of G–K stars, but only for 6% of M stars (when using a coordinate matching radius of 2'')<sup>3</sup>. We fitted each distribution of proper motions (in RA\*cos(Dec) and Dec) with a Gaussian to get a mean of  $-4.6$  mas/yr and  $5.7$  mas/yr, and  $\sigma$  of  $5.0$  and  $4.8$  mas/yr, respectively. Objects with proper motion vectors within 10 mas/yr ( $2\sigma$ ) of the cluster mean have been marked as members (flag “Y” in the last column of Tables 1 and 2). Objects more than 10 mas/yr from the mean are marked as proper motion non-members. We find the proper-motion-confirmed member fraction to be 95%, 81%, 52%, 77% and 80% among BA, F, G, K, and M-type photometric members, respectively.

## 4. IDENTIFYING EXCESS CANDIDATES

<sup>2</sup> Also available via the VizieR Online Data Catalogs I/289 and I/294.

<sup>3</sup> Spectral classes are assigned based on  $(V - K)_0$  or on  $(R - K)_0$  color when the former is not available, following Bessell & Brett (1988) and Kenyon & Hartmann (1995) dwarf calibrations. Reddening  $E(B - V) = 0.06$  and following relations were adopted for all NGC 2547 stars:  $A_V = 3.1E(B - V) = A_R/0.748 = A_K/0.112 = A_{[5.8]}/0.048 = A_{[8]}/0.048 = A_{[24]}/0.0$

#### 4.1. *IRAC Excesses*

The four IRAC bands spanning 3-8  $\mu\text{m}$  trace dust from the near-sublimation temperature of  $\sim 1000$  K to about 400 K, corresponding to radii within 1 AU for solar-type stars. To identify possible 8  $\mu\text{m}$  excesses from the IRAC data, we plot sources from Tables 1 and 2 on the  $V - K$  vs  $K - [8]$  diagram in Figure 6. The large baseline of the  $V - K$  color results in a monotonic relationship between increasing redness and increasingly late stellar spectral type. For stars with no excess, the similarity of the photospheric colors for a given spectral type results in a narrow locus, extending from  $V - K \sim 0$  (for A-type and earlier stars) to 5 (early M); the scatter in this locus increases for  $V - K > 5$  due to measurement errors. Stars to the right of this locus are candidates to have excesses at 8  $\mu\text{m}$ .

We visually examined the quality of the image of each object with an apparent 8  $\mu\text{m}$  excess. We removed nine objects from the plot because of a nearby companion, cosmic ray hit, artifact from a bright star, or a non-uniform nebulosity contaminating the 4 px-wide aperture. One more object (2MASS 08104684-4927452) was rejected because it was too faint on the  $V$  vs  $V - K$  diagram. Four more were not plotted because they had non-stellar flags on the  $RIZ$  magnitudes. Only one of these 14 objects is detected at 24  $\mu\text{m}$  (2MASS 08100961-4915540), and its 24  $\mu\text{m}$  excess is in question as well, due to strong nebulosity. All these sources were omitted from Fig. 6.

A similar diagram was constructed in the  $R - K$  color (Fig. 7). We omitted the objects excluded from Fig. 6 plus nine additional objects (none of which has a  $V$  mag) with questionable 8  $\mu\text{m}$  excesses due to poor image quality. One more (2MASS 08111674-4906564) was rejected because it is too faint on the  $R$  vs  $R - K$  diagram. Of these 10 objects only one is detected at 24  $\mu\text{m}$ , with only marginal excess due to closeness to the detection limit (2MASS 08090351-4909148). Tables 1 and 2 include footnotes regarding source selection issues.

The remaining 8  $\mu\text{m}$  excesses were marked with numbers on Figures 6 and 7. Excess objects were visually selected by being  $\geq 3\sigma$  away from the average locus formed by the majority of members of the corresponding  $V - K$  ( $R - K$ ) color. The 8  $\mu\text{m}$  channel is significantly affected by the cosmic ray hits. Since the size of the IRAC beam is only about 4 pixels, for faint objects it is sometimes difficult to decide whether a detection is real or an artifact of a cosmic ray hit. However, if an excess is found at 8  $\mu\text{m}$ , we can expect to detect it also in the 5.8  $\mu\text{m}$  band. We therefore constructed  $V - K$  vs  $K - [5.8]$ ,  $R - K$  vs  $K - [5.8]$  diagrams (Figs 8, 9). As can be seen from these plots, most faint members with 8  $\mu\text{m}$  excesses do not stand out at 5.8  $\mu\text{m}$ : ID 3 (2MASS 08104343-4930158), 5 (2MASS 08085856-4911171), 6 (2MASS 08101041-4858052), 7 (2MASS 08093547-4913033), 10 (2MASS 08104401-4859372), 11 (2MASS 08083389-4907176), 12 (2MASS 08094287-4903413). To guard against bad photometry due to cosmic ray hits, we required an excess in faint sources to be apparent at both 5.8 and 8  $\mu\text{m}$ . In the absence of additional information about objects rejected based on this requirement we do not discuss them further, with the exception of ID 7, which was already noticed by Young et al. (2004) to have a 24  $\mu\text{m}$  excess

and for which we obtained a spectrum. Properties of ID 7 together with the remaining 8  $\mu\text{m}$  excess objects are presented in Table 5.

#### 4.2. *MIPS Excesses*

The cluster has mass segregation, with members above 2  $M_\odot$  (mid-Fs) all gathered within the central 20' (Littlefair et al. 2003; Jeffries et al. 2004). This mass limit coincides with the limit for photospheric detection at 24  $\mu\text{m}$ , which is at  $\sim 10.8''$ , or 0.3 mJy (where the distribution of [24] magnitudes experiences a sharp downturn). We can achieve excess *detections* to lower masses, but we will be unable to calculate the excess *fraction* (the fraction of stars with excess) there. Thus, compared to Young et al. (2004), we are probing the disk fraction at 24  $\mu\text{m}$  to a similar (stellar) mass limit. The advantage of our study is improved statistics for excess detections down to early M stars, due to the larger area covered; as a result, we detect a few sources with excesses even more extreme than in Young et al. (2004) (§5).

How do we identify 24  $\mu\text{m}$  excesses? The cluster is young and has a continuum of objects with  $K - [24]$  bigger than  $\sim 0$  expected from the Rayleigh-Jeans tail of the pure photospheric emission for stars earlier than early M (Figs. 10, 11). The non-excess locus thus cannot be easily identified from the stars of NGC 2547 itself. We therefore use the Pleiades locus as a fiducial. One can see that all the NGC 2547 stars fall inside or to the right of the adopted non-excess boundaries relative to this locus. We regard objects  $3\sigma$  to the red relative to the central line to have a 24  $\mu\text{m}$  excess and report them in Table 5. To reproduce the Pleiades locus in the  $R - K$  color in Fig. 11, we used the relation between  $R - K$  and  $V - K$  for B9-K7 MS stars from Kenyon & Hartmann (1995). Two new excesses are identified on this diagram, with  $K - [24]$  between 1.5 and 2 mag.

The five optically brightest members (B stars) formally show excess at 24  $\mu\text{m}$ , but in all of them the emission is extended beyond the 6''-wide MIPS beam, corresponding to 2400 AU at 400 pc. This scale is too big for a typical debris disk. The behavior was first encountered in follow-up studies of *IRAS*-discovered excesses, and was dubbed “the Pleiades phenomenon”. It is explained by accumulation of matter around massive stars as a result of either mass loss or the radiation pressure exerted on the interstellar dust, and should not be confused with a debris disk that results from the shattering of planetesimals. Indeed, two bubbles are seen on Fig. 1 around these “halo” stars. The bigger one in the northern part of the cluster is centered on the B5 II member HD 68451, and the more compact one in the center of the cluster is clearly produced by the B3 IV star HD 68478. We mark these stars in Table 1 and omit them from the  $K - [24]$  plots.

At magnitudes near the detection limit one has to worry about confusion with ISM clumps and extragalactic objects. We examined the images of all 24  $\mu\text{m}$  excess sources. To help the discussion and guide the eye on Fig. 10, we split these objects into several groups based on  $V - K$  (see Table 5). Three of the four excess sources with  $V - K \sim 1.6$  and  $K - [24] = 0.6 - 0.9$  have distorted shapes, while 6 sources out of 8 with  $V - K > 2.5$  ( $R - K > 1.8$ ),  $K - [24] = 0.6 - 4$  are at the level of fluctuations in the nebulosity. We

therefore call these excesses “possible”. We note that the region of  $V - K = 2 - 4$  is also where contamination from background giants is strongest (Littlefair et al. 2003). Indeed, 2MASS 08101474-4912320, whose membership is only based on *BVI* photometry, has a radial velocity  $> 100$  km/s which is much larger than the cluster mean (§3.2). We do not discuss objects from this group any further. The images of the remaining excess sources however (including the four most extreme ones with  $K - [24] > 3.5$ ) appear symmetrical, and where radial velocities are measured, they are consistent with cluster membership. We discuss them in §5.

## 5. PROPERTIES OF THE EXCESS CANDIDATES

### 5.1. $8 \mu\text{m}$ excesses

Sources with excesses at  $8 \mu\text{m}$  are rare in this cluster. We discuss the characteristics of each of them below.

*ID 1* has only a marginal excess at  $8 \mu\text{m}$  and has a border-line one at  $24 \mu\text{m}$ . The RV and proper motion are consistent with membership. The weak excess may arise from the ISM nebulosity affecting the photometry.

*ID 2* shows only marginal excess at  $8 \mu\text{m}$  but a significant level in the NIR and at  $24 \mu\text{m}$ . It is a highly probable member according to its proper motion. We resolved it into two objects  $1''$  apart. The system is entered in the Washington Visual Double Star Catalog (Worley & Douglass 1997) with only three observations from 1929-1949, leaving open the question of the physical association of the objects. Our spectrum of the primary is consistent with late A7-A9 reported in the literature, and the radial velocity is close to the cluster mean. The secondary has stronger Ca II lines, lacks Pa lines and a radial velocity larger by 23 km/s. We speculate that it may be a background K giant, which would explain the anomalous  $H - K$  color of the system. Does the  $24 \mu\text{m}$  excess originate from the primary A type member or the K giant then? We are inclined to attribute it to the former since excesses around G-K giants are rare (Zuckerman, Kim & Liu 1995; Jura 1990; Plets et al. 1997), while excesses around A stars of this age are very common (Rieke et al. 2005).

*ID 4* in Jeffries et al. (2003) is indicated as a K5 radial velocity member with Li absorption and weak chromospheric emission in  $\text{H}\alpha$  (RX 9). It is interesting that besides a weak  $8 \mu\text{m}$  excess it also shows a robust excess at  $4.5 \mu\text{m}$  and a marginal one at 3.5 and  $5.8 \mu\text{m}$ . We did not obtain a spectrum of it.

*ID 7* is the latest-type member with a robust detection at  $24 \mu\text{m}$ , indicating an excess of  $\sim 3$  mag. It was the largest excess detected in Young et al. (2004). Jeffries & Oliveira (2005) classified it as an M4.5 radial velocity member with no Li. It does not show excess at  $5.8 \mu\text{m}$ , but has the reddest  $K - [8]$  color among late-type members (we do not count ID 12 as a reliable detection). The strong K I at  $7699\text{\AA}$  and Na I doublet at  $8200\text{\AA}$  in our spectrum firmly rule out the possibility of a low-gravity background giant (Torres-Dodgen & Weaver 1993; Schiavon et al. 1997), while our radial velocity again confirms membership. The spectrum shows emission in  $\text{H}\delta$  and  $\text{H}\gamma$ , but higher resolution is needed to tell whether the emission is due to a chromosphere or to accretion. The  $24 \mu\text{m}$  excess of *ID 7* is surpassed by only one other candidate M-type member, 2MASS 08090344-

4859210 (Fig. 10). With  $F_{24} = 1.2$  mJy, this source is a clear detection despite the expected low mass. It makes a close match with *ID 7* in optical colors, being only 0.15 mag bluer in  $R - I$  and  $V - K$ , indicating a spectral type of  $\sim \text{M}3$ . Similarly to *ID 7*, the excess vanishes in the shorter IRAC bands. If this object is a sibling of *ID 7*, it would mean that stars of  $\sim 30$  Myr age and  $\sim 0.25 M_{\odot}$  are capable of generating dusty disks even more vigorously than massive stars. There is a caveat though. Jeffries et al. (2004) dismiss it as a member based on the *RIZ* photometry. However, it is only 0.05 mag off the nearest members on the  $I$  vs  $R - I$  and  $I - Z$  vs  $R - I$  diagrams, and is a legitimate member on  $I$  vs  $I - Z$ ,  $V$  vs  $V - K$  ( $R - K$ ,  $I - K$ ) color-magnitude diagrams. With  $J - H = 0.76 \pm 0.06$ ,  $H - K = 0.25 \pm 0.06$  it is slightly above other late type members on the  $J - H$  vs  $H - K$  diagram, with errorbars allowing either a dwarf or a giant interpretation. Spectroscopy of gravity-sensitive features similar to that for *ID 7* is needed to resolve this interesting case.

*ID 8* is a single mid-G member according to the optical and NIR color-magnitude diagrams. Our spectrum is consistent with this classification and indicates that its radial velocity is also consistent with membership. Together with *ID 9*, it is unique in that its excess starts already at  $3 \mu\text{m}$ .

*ID 9* has the biggest excesses at all IRAC wavelengths and at  $24 \mu\text{m}$  in our survey. It was detected already by *IRAS*; the Serendipitous Survey Catalog (Kleinmann et al. 1986) contains a measurement at  $25 \mu\text{m}$  and upper limits at 12 and  $60 \mu\text{m}$ . The *IRAS* flux at  $25 \mu\text{m}$  is in excellent agreement with ours: 0.16 Jy. According to the *VRK* color-magnitude diagrams, it could be an equal-mass binary late-K dwarf. Our spectrum is consistent with this classification. The radial velocity of  $+29$  km/s is consistent with membership, being within the HWHM from the cluster value in its radial velocity group (Fig. 5). The only notable difference between it and the other members with similar colors is the shallower and broader lines, indicating faster than typical rotation with  $v \sin i > 20$  km/s (see Fig. 4 in Jeffries, Totten, & James (2000)). Its  $H - K$  color of 0.3 mag is however more characteristic of a mid-M dwarf. We can rule out the latter classification with our spectrum. It appears therefore that *ID 9* has an IR excess starting at  $2 \mu\text{m}$  and rising all the way to  $24 \mu\text{m}$ .

The fraction of  $8 \mu\text{m}$  excesses for all sources in Tables 1 and 2 except for those with peculiarities discussed in footnotes is  $< 5\%$  (0/20),  $\leq 7\%$  (0 - 2 out of 28, depending on the marginal cases of *ID 1* and *ID 2*), 1.5% (1/68), 1.0% (2/208), and 0.4% (1/227) for BA, F, G, K and M stars respectively. When discarding proper motion non-members and applying the proper motion membership fraction found in §3.3 to those without proper motion estimates, we obtain correspondingly  $< 5\%$  (0/19),  $\leq 9\%$  (0-2/23), 2.6% (1/(35+7×0.52)), 1.2% (2/(143+30×0.77)),  $\leq 0.6\%$  ( $\leq 1/(8+216×0.80^4)$ , depending on whether *ID 7* is a proper motion member or not). Summarizing, we find the  $8 \mu\text{m}$  excess fraction at 30 Myr to be  $\sim 1\%$  for

<sup>4</sup> Though high membership probability for M stars in NGC2547 is based on only 21 stars with known proper motions, it was confirmed in the RV and Li study of Jeffries & Oliveira (2005) with three times larger sample.

the intermediate-mass to low-mass stars. Among four detected 8  $\mu\text{m}$  excesses two (ID 4, ID 7) are weak and two (ID 8, 9) are highly significant; three of them also have detected 24  $\mu\text{m}$  excesses.

### 5.2. 24 $\mu\text{m}$ excesses

Excesses at 24  $\mu\text{m}$  are far more common than at 8  $\mu\text{m}$ . There are 27 objects in Table 5 that show excess at the former but not at the latter wavelength. To compare NGC 2547 to other (mostly older) clusters, we compute the fraction of members with 24  $\mu\text{m}$  excess. As we have seen, by  $(V - K)_0 \sim 1.4$  we start missing members in the MIPS band, while the identified excesses are prone to confusion with unrelated sources and nebulosity. We therefore calculate the excess fractions below this limit. In the range  $-0.2 \leq (V - K)_0 < 0.7$ , corresponding to  $\sim\text{B8-A9}$ , 8 out of 18 highly probable members with good photometry show excess, resulting in an excess fraction of 44%. Adding 2 possible members of which one has excess (triangles on Fig.10) results in 45% (9 out of 20). All these sources are also proper motion members, except for non-excess 2MASS 08094610-4914270, which however qualifies as member based on the Tycho Catalog measurement<sup>5</sup>. In the range of  $0.7 \leq (V - K)_0 < 1.4$ , F0-F9, the excess fraction among the highly probable photometric members is 33% (7/21) and the same (33%) with addition of 3 possible members (8/24). Excluding 4 proper motion non-members, all of which are non-excess stars, increases the excess fraction in F stars to 40% (8/20).

## 6. DISCUSSION

### 6.1. Evolution of 8 micron excess

The inner accretion disks have been extensively studied at 2–4  $\mu\text{m}$  already from the ground, and the colder debris disks at 24–70  $\mu\text{m}$  in the recent large *Spitzer* surveys (e.g., Kim et al. 2005; Rieke et al. 2005; Bryden et al. 2006; Su et al. 2006; Meyer et al. 2007)). Recent *Spitzer* studies are also starting to put together a picture of the evolution of inner disks probed at 8  $\mu\text{m}$ .

Emission at 8  $\mu\text{m}$  traces dust hotter than  $\sim 300$  K, corresponding to distances of  $\sim 1$ –10 AU around G–A stars, and  $\sim 0.1$ –1 AU around M–K stars. Non-detection of 8  $\mu\text{m}$  excess in the majority of NGC 2547 members signals a thorough cleaning of hot dust by 30 Myr. Assuming that grains emitting at 8  $\mu\text{m}$  are astronomical silicates with a dust temperature of 350 K, grain density of 2.5 g  $\text{cm}^{-3}$  and a radius of 10  $\mu\text{m}$ , a 8  $\mu\text{m}$  excess of 0.1 mag around A–F type stars corresponds to a dust mass of  $\sim 10^{-4} M_{\text{Moon}}$ , and  $\sim 10^{-5} M_{\text{Moon}}$  for an excess of 0.15 mag around G to early-M stars in NGC 2547.

Excess at 8  $\mu\text{m}$  is generally found in young stars simultaneously with excesses at shorter IRAC bands and at 24  $\mu\text{m}$ , implying presence of optically thick primordial disks. Stars with colors close to photospheric in the shorter IRAC bands but with excesses starting at  $\sim 8$ –10  $\mu\text{m}$  are less frequent. In stars several Myr old such disks are called “transition”, meaning they can be in the evolutionary state from primordial to debris (e.g., Hartmann et al. 2005a; Lada et al. 2006). The reduced emission in the IRAC bands is interpreted as either grain

growth/settling or clearing by the dynamical effects of giant planets. Depending on the excess at longer wavelengths, further subdivision of transition disks can be found in the literature. It is also possible that some of the transition-like SEDs may actually belong to young debris systems (Currie et al. 2007a; Furlan et al. 2007; Hernández et al. 2007; Rhee et al. 2007).

Hernández et al. (2006) surveyed 60 B–F stars in the two Orion subassociations OB1b (5 Myr old) and OB1a (10 Myr old). They found two 8  $\mu\text{m}$  excesses in the younger group (one arising from the accretion disk of a Herbig Ae star and another from a massive debris), and one excess in the older group (from a Herbig Ae star), resulting in 8  $\mu\text{m}$  excess fractions among hot stars of 9% and 5% at 5 and 10 Myr respectively. Sicilia-Aguilar et al. (2006) studied two clusters in Cepheus OB2 association. Among 21 B–F stars with 8  $\mu\text{m}$  measurements in the 4 Myr old Tr 37, two show excesses, only one of which may be due to a dusty disk (the other star is of the classical Be type). In the 10 Myr old NGC 7160 2 out of 68 stars show weak 8  $\mu\text{m}$  excesses. These fractions, 5–10% at 4 Myr and 3% at 10 Myr are quite consistent with the Orion results, indicating a fast decline of 8  $\mu\text{m}$  emission in massive stars. The fraction of G–M stars with measured 8  $\mu\text{m}$  excess is much higher:  $\sim 60\%$  (of which 15% are classified as transitional) in Tr 37 and 5–8% in NGC 7160 (1–2 of excesses are transitional and the other one is primordial).

Megeath et al. (2005) studied 15 K–M stars in the  $\eta$  Chameleon 5–9 Myr association. They found 6 to have excesses at the IRAC bands (excess fraction 40%), five of these are accretors, one not. None of the two A members shows excess. Low et al. (2005) summarize SEDs for the 8–10 Myr old TW Hydriæ association. Among 22 K–M members, 3 show excesses at 8–10  $\mu\text{m}$ , two of which are from primordial disks (TW Hya and Hen 3-600) and one from a debris disk (HD 98800AB), resulting in an excess fraction of 14%. Currie et al. (2007b) found in the 13 Myr-old double cluster  $\chi$  &  $h$  Persei 8  $\mu\text{m}$  excesses in 1–3% of the intermediate-mass stars and up to 4–8% in the solar-mass stars (at their completeness limit of 1.2–1.4  $M_{\odot}$ ). Silverstone et al. (2006) surveyed 74 solar-mass (G–mid-K) young nearby stars with IRAC and MIPS. They found 5 stars with IRAC excesses, all of them from optically-thick disks; all are younger than 20 Myr. The excess fractions are  $14_{-7}^{+11}\%$  and  $2_{-2}^{+5}\%$  for the 3–10 Myr and 10–30 Myr bins respectively.

Although there is some scatter (probably in part due to statistical uncertainties in relatively small samples), these studies agree on a dramatic overall decay in 8  $\mu\text{m}$  excess incidence over the first 20 Myr of stellar evolution. Beyond this age such excesses become very uncommon, and based on the dynamic arguments of the grain survival time are expected to have debris origin. At 30 Myr among  $\sim 500$  B–M stars in NGC 2547 we identify 4 with IRAC excesses, two of which are only marginal, while the other two are extremely strong (§6.2). Mamajek et al. (2004) studied 14 F–M members of the 30 Myr old Tucana-Horologium association and found none with 10  $\mu\text{m}$  excess, resulting in an excess fraction  $< 7\%$ . The less homogeneous *Spitzer* studies of field stars have yielded only a few discoveries of hot disks beyond 30 Myr. Chen et al. (2006) obtained *Spitzer* IRS

<sup>5</sup> Available via the VizieR Online Data Catalog I/250.

spectra for 59 nearby mostly B–F stars with *IRAS* 60  $\mu\text{m}$  excesses. They found 7 at ages  $\leq 10$  Myr, 2 at ages 20–50 Myr and 2 at 500–1000 Myr ( $\zeta$  Lep and  $\eta$  Crv) to have 8–13  $\mu\text{m}$  excess (in amount  $\geq 10\%$  above the photospheric flux). From a similar study of 41 main sequence F5–K5 stars Beichman et al. (2006) found another two (HD 69830 and HD 72905), only one of which is older than 1 Gyr, resulting in an excess fraction of 2.5% among old stars. Uzpen et al. (2005, 2006) searched the MSX and the GLIMPSE *Spitzer* Legacy Program fields in the Galactic plane for excess due to hot circumstellar disks. They found  $\sim 50$  such candidates among B–K field stars. Unfortunately we can not include them in our analysis due to the lack of information about their ages, but a significant proportion show signs of youth (Uzpen et al. 2006).

As we have seen, unlike the shorter IRAC wavebands, the 8  $\mu\text{m}$  excess can trace both primordial and debris material, and therefore should be used in combination with other diagnostics to interpret its overall decay with age. The above studies indicate an inside-out evolution for *primordial* disks. The inner-most parts of the disks (within few stellar radii), as traced by the NIR photometry and spectroscopic signatures of accretion, clear out on a time scale of  $\sim 3$  Myr, with the disk fraction falling by 10 Myr to a few percent for solar-mass stars and essentially to zero for intermediate-mass ones. Excess at 6–8  $\mu\text{m}$  holds longer, being at a level of 5–10% for low-mass stars at 10 Myr and dropping to 1% by 30 Myr. The evolution of *debris* disks is more slowly, with a characteristic time scale of 150 Myr for the 24  $\mu\text{m}$  excess (Rieke et al. 2005; Gorlova et al. 2006; Siegler et al. 2006; Su et al. 2006) and  $\sim 400$  Myr for 70  $\mu\text{m}$  (Su et al. 2006). The collisional cascades beyond 10 Myr are maintained with the formation of the large icy bodies in the outer disk that are capable to steer leftover planetesimals (Dominik & Decin 2003; Kenyon & Bromley 2004b, 2005; Hernández et al. 2006). Unlike 24  $\mu\text{m}$  excess, 8  $\mu\text{m}$  excess does not show a secondary peak after first few Myrs, and is less frequent among B–A stars. This behavior may imply a rapid depletion of the material within 1 AU, inhibiting planet formation and the corresponding debris stage in this radial zone. Even if planets do form in a few Myr, as rare cases with inner holes suggest, the end process of planet formation in this zone must lead to the rapid dissipation of smaller bodies to inhibit collisional cascades (e.g., due to the absence of icy bodies or because of the rapid inward planet migration (Burkert & Ida 2006)).

## 6.2. Transitional disks at 30 Myr?

De-reddened spectral energy distributions of NGC 2547 sources with 8  $\mu\text{m}$  excess are presented in Fig. 12. First we over-plot Kurucz models with effective temperatures corresponding to the expected spectral types and sub-giant gravity, normalizing them to fit the observations in the J band. The flux beyond 10  $\mu\text{m}$  was extrapolated with the Planck function. As one can see, photospheric models match the SEDs of the excess stars well from 0.4 (B band) to 2  $\mu\text{m}$  (K), with only a slightly worse fit for ID 7 (M4.5) with strong molecular features. These fits confirm that excess emission is present in all *Spitzer* bands in ID 8 and 9, and starts at 8  $\mu\text{m}$  in ID 7, a result we obtained previously from empirical color–color diagrams. We fit the excess emission with a series

of black bodies, by varying the temperature and the normalization factor. The best fits together with the fraction of the excess flux relative to the photospheric value  $\tau$  ( $= L_{Exc}/L_{*Bol}$ ) are given in Fig. 12. For comparison, we also show the median SED for the low-mass stars with optically-thick disks in the 1–2 Myr-old Taurus region (D’Alessio et al. 1999; Hartmann et al. 2005a). We could not obtain a satisfactory single-temperature fit for ID 9, so a 250 K black body curve is shown for reference only. For ID 4 the small IRAC excesses and the low upper limit on 24  $\mu\text{m}$  flux require temperature for excess emission of no less than 1000 K. The best fit is achieved with a maximum possible temperature of 1500 K, corresponding to dust sublimation temperature. While the fractional excess luminosities of ID 4 and 7 place them in the range of typical debris systems, the luminosities of ID 8 and 9 are too big, suggesting that at least ID 9 must have an optically-thick disk.

Three possibilities exist to explain the excesses of ID 8 and 9: 1) the disks are transitional, evolving from primordial to debris (as seen in the smaller IRAC excesses compared to Taurus), 2) a catastrophic collision occurred between two planetary-size bodies, 3) these objects are background post-MS stars experiencing mass-loss.

The 3.5–5.8  $\mu\text{m}$  colors of both ID 8 and 9 are consistent with colors of classical T Tau stars (CTTS) (Hartmann et al. 2005a). The 8 and 24  $\mu\text{m}$  excesses of ID 8 are also more characteristic of CTTS and only rarely observed in weak T Tau stars, while the excesses of ID 9 are extreme even for CTTS (Padgett et al. 2006). Despite big mid-IR excesses, the two stars however lack strong excess in the NIR (ID 8 has none). They also lack emission for example in H $\delta$  and the Ca II triplet in our spectra. These are characteristics of transitional disks where gas accretion has ceased and dust has dissipated from the inner 0.1 AU, but primordial dust at larger radii is still present. The question is whether the 30 Myr age of the cluster is widely discrepant with this interpretation. The typical ages of T Tau and transitional disks are a few Myr. On the other hand, K-band excess may persist at the level of few percent at ages of 10 Myr (Hillenbrand 2005; Bonatto et al. 2006). The cases of gas accretion beyond 10 Myr are rare but also exist, the most famous being a low-mass Classical T Tau star St 34 in the Taurus, whose Li age is at least 25 Myr according to White & Hillenbrand (2005) and Hartmann et al. (2005b). They suggest that the long-lived accretion is maintained due to binarity of this star with sub-AU separation. ID 8 does not appear to be a binary though. The nearby associations like TW Hya and  $\eta$  Cha present the best examples of how diverse disks can be at 10 Myr (Low et al. 2005; Riaz, Gizis, & Hmiel 2006; Megeath et al. 2005). Considering that our study is one of the first that explore disks at 0.1–1 AU at the 20–40 Myr age range with good statistics, we can not dismiss the possibility that ID 8 and 9 may be the oldest known transitional disks around solar-mass stars.

Interesting, NGC 2547 is at a similar era when the Earth–Moon system formed. It is believed that the Earth–Moon system resulted from a giant impact between the proto-Earth and a Mars-sized body (Canup 2004). After the impact, it is thought that the proto-Earth accreted less than 5% of a current Earth mass from the impactor, while  $\sim 30\%$  of the impactor mass was va-

porized and escaped. Only 1.5 to 2  $M_{Moon}$  of material stayed bound to the proto-Earth orbit, forming a disk around the Earth that eventually consolidated into the Moon. We have explored whether such a giant impact might be responsible for the infrared excess we observe around ID 8. Using an optically thin disk model with the assumptions of constant surface density and a power-law grain size distribution ( $\Delta N \sim a^{-3.5} \Delta a$ ) of astronomical silicates, the 8 and 24  $\mu\text{m}$  excesses are consistent with a disk with an inner radius of  $\sim 0.1$  AU (dust sublimation radius for 0.1  $\mu\text{m}$  grains) and an outer radius of  $\sim 1$  AU. A wide range of grain size distributions can yield reasonable fits to the data, but all the fits require a dust mass on the order of  $10^{-3} M_{Moon}$ . The mass we derived here is a lower mass limit of the total material around ID 8 since we used an optically thin model. In addition, the mid-infrared observations do not trace the population of large (km-size) parent bodies. Following the same approach as for HD 69830 by Beichman et al. (2005), we estimate a total mass of parent bodies on the order of 3–10  $M_{Moon}$ , assuming the maximum size of the parent bodies is 1 to 10 km.

Could ID 8 & 9 be interpreted as background interlopers with dusty envelopes? Indeed, ID 9 is in the region of the cluster color-magnitude sequence that is most strongly contaminated by Galactic G–K giants (Littlefair et al. 2003). ID 8 is not, but it comfortably lies among dusty evolved stars on the [3.5] – [8] vs. [8] – [24] diagram of the LMC field in Meixner et al. (2006). Despite their big mid-IR excess, the  $H - K$  excess in ID 8 and 9 is much weaker compared with the AGB stars (Buchanan et al. 2006). Perhaps ID 8 and 9 then belong to a rare class of the first-ascent G–K giants where IR excess originates from a shell thrown off as a result of a mixing event in the stellar interior (de La Reza, Drake, & da Silva 1996; Drake et al. 2005)? CO first-overtone bands at 2.3  $\mu\text{m}$  can be used to probe the background giant explanation for ID 8 and 9 from low-resolution spectra. This feature appears at spectral type mid-G and strengthens at lower temperatures. It is also strongly gravity-sensitive, for the same spectral type being deeper in supergiants and giants ( $\log g \leq 3$ ) than in dwarfs ( $\log g \sim 4.5$ ) (Kleinmann et al. 1986; Wallace & Hinkle 1997; Ivanov et al. 2004). According to the evolutionary models (Siess et al. 2000), G–K stars in NGC 2547 are close enough to the Main Sequence to have dwarf gravities within a few tenths of a dex; therefore, the CO band should be weak in them. In Fig. 13 we show our K-band spectra of ID 8 & 9 overplotted on the spectra of field stars from Kleinmann et al. (1986)<sup>6</sup>, and a spectrum of HIP 43141A obtained and reduced by us in the same manner as ID 8 & 9. The spectra of ID 8 & 9 lack strong features, consistent with G to mid-K spectral types expected from observed colors and negligible extinction in the cluster. ID 8 shows a weak but distinctive  $\text{Br}\gamma$  line, indicating an earlier SpT than ID 9. ID 9 in turn clearly shows a CO(2,0) band-head at 2.294  $\mu\text{m}$ , which best compares with the K5 dwarf 61 Cyg A. Despite residual telluric noise in that region,

we can firmly rule out any possibility for ID 8 & 9 to be common late K – M giants. However at this low resolution we can not exclude possibility of ID 8 & 9 being mass-losing G supergiants, with simultaneously shallow  $\text{Br}\gamma$  and CO lines due to filling emission and residuals induced in the telluric correction process. Such stars are however extremely rare (Oudmaijer et al. 1995). In summary, the near-IR spectra of ID 8 & 9 are consistent with a mid-G and mid-K dwarf types respectively, supporting their membership in the cluster.

## 7. CONCLUSIONS

We have extended the survey of Young et al. (2004) of the circumstellar disks in the 30 Myr old cluster NGC 2547 to include the newly identified members over the entire  $1.5^\circ \times 1^\circ$  area covered by *Spitzer*. Among  $\sim 600$  B–mid-M probable members (corresponding to masses down to  $0.2 M_\odot$ ) where we are sensitive to the photospheric level, only 4 stars show convincing excesses in the IRAC bands, corresponding to an excess fraction  $\lesssim 1\%$ . This behavior is in striking contrast with the 24  $\mu\text{m}$  excesses exhibited by 30–45% of the B–F members.

Of the four 8  $\mu\text{m}$  excesses, two are marginal and have SEDs consistent with debris disks (around an M4 dwarf discovered by Young et al. (2004) and a K5 dwarf). The other two members have strong 8  $\mu\text{m}$  excesses. One is a mid-G dwarf with SED consistent with a massive hot debris disk, perhaps the result of a giant impact. Another is a mid-K dwarf whose SED is more consistent with an optically-thick disk, though with depressed 2–6  $\mu\text{m}$  emission compared with the average SED of a CTTS. Though we do not find signatures of gas accretion in our spectra of these two stars, spectroscopic investigation at higher resolution is needed to confirm the transitional nature of these disks. We identify another possible mid-M member with excess starting between 8–24  $\mu\text{m}$ ; if confirmed, it will be one of the few known M dwarfs older than 20 Myr with mid-IR excess (Siegler et al. 2006).

Our survey provides the best evidence to date that the frequency of the 8  $\mu\text{m}$  excess that traces the disk zone inside  $\sim 1$  AU around solar-type stars diminishes to less than  $\sim 1\%$  by 30 Myr. If planetary formation occurs inside 1 AU, it must be complete by 30 Myrs.

We would like to thank J. Harris, D. Kelson, A. Oemler, G. Walth and Y. Yang for help with IMACS reduction, and J. S. Kim and N. Siegler for help with observations. An anonymous referee provided many insightful comments. This paper includes data gathered with the 6.5 meter Magellan Telescopes located at Las Campanas Observatory, Chile. This publication makes use of data products from the Two Micron All Sky Survey, which is a joint project of the University of Massachusetts and the Infrared Processing and Analysis Center/California Institute of Technology, funded by the National Aeronautics and Space Administration and the National Science Foundation. This work was supported by JPL/Caltech under contract 1255094.

<sup>6</sup> Available in the electronic form from the VizieR on-line catalog III/114

## REFERENCES

Allen, L. E. & Strom, K. M. 1995, AJ, 109, 1379  
 Baraffe, I., Chabrier, G., Allard, F., & Hauschildt, P. H. 2002, A&A, 382, 563

Beichman, C. A., et al. 2005, *ApJ*, 626, 1061

Beichman, C. A., Tanner, A., Bryden, G., Stapelfeldt, K. R., Werner, M. W., Rieke, G. H., Trilling, D. E., Lawler, S., & Gautier, T. N. 2006, *ApJ*, 639, 1166

Bessell, M. S. & Brett, J. M. 1988, *PASP*, 100, 1134

Bonatto, C., Bica, E., Ortolani, S., & Barbuy, B. 2006, *A&A*, 453, 121

Bryden, G. et al. 2006, *ApJ*, 636, 1098

Buchanan, C. L., Kastner, J. H., Forrest, W. J., Hrivnak, B. J., Sahai, R., Egan, M., Frank, A., & Barnbaum, C. 2006, *AJ*, in press (astro-ph/0606756)

Burkert, A. & Ida, S. 2006, *ApJ*, submitted (astro-ph/0608347)

Canup, R. M. 2004, *ARA&A*, 42, 441

Carquillat, J. M., Jaschek, C., Jaschek, M., & Ginestet, N. 1997, *A&AS*, 123, 5

Chambers, J. E. 2001, *Icarus*, 152, 205

Chen, C. H. et al. 2006, *ApJS*, in press (astro-ph/0605277)

Clariá, J. J. 1982, *A&AS*, 47, 323

Currie, T., Kenyon, S., Rieke, G., Balog, Z., & Bromley, B. C. 2007a, *ApJ*, in press (astro-ph/0706.0535)

Currie, T., Balog, Z., Kenyon, S. J., Rieke, G., Prato, L., Muzerolle, J., & Young, E. T. 2007b, *ApJ*, 659, 599

D'Alessio, P., Calvet, N., Hartmann, L., Lizano, S., & Cantó, J. 1999, *ApJ*, 527, 893

D'Antona, F. & Mazzitelli, I. 1997, *Mem. Soc. Astron. Ital.*, 68, 807

de La Reza, R., Drake, N. A., & da Silva, L. 1996, *ApJ*, 456, L115

Dias W.S., Florio, V., Assafin M., Alessi B.S., Libero V. 2006, *A&A*, 446, 949

Dominik, C. & Decin, G. 2003, *ApJ*, 598, 626

Drake, N. A., de la Reza, R., da Silva, L., & Lambert, D. L. 2002, *AJ*, 123, 2703

Furlan, E. et al. 2007, *ApJin* press (astro-ph/0705.0380)

Gorlova, N. et al. 2004, *ApJS*, 154, 448

Gorlova, N., Rieke, G., Muzerolle, J., Stauffer, J., Siegler, N., Young, E., & Stansberry, J. 2006, *ApJ*, in press (astro-ph/0606039)

Gutermuth, R. A., Megeath, S. T., Muzerolle, J., Allen, L. E., Pipher, J. L., Myers, P. C., & Fazio, G. G. 2004, *ApJS*, 154, 374

Hanson, M. M., Conti, P. S., & Rieke, M. J. 1996, *ApJS*, 107, 281

Hartmann, L., Megeath, S. T., Allen, L., Luhman, K., Calvet, N., D'Alessio, P., Franco-Hernandez, R., & Fazio, G. 2005a, *ApJ*, 629, 881

Hartmann, L. et al. 2005b, *ApJ*, 628, 147

Hernández, J. et al. 2005, *ApJ*, 129, 856

Hernández, J., Briceño, C., Calvet, N., Hartmann, L., Muzerolle, J., & Quintero, A. 2006, *ApJ*, in press (astro-ph/0607562)

Hernández, J. et al. 2007, *ApJ*, 662, 1067

Hillenbrand, L. A. 2005, "A Decade of Discovery: Planets Around Other Stars" STScI Symposium Series 19, ed. M. Livio (astro-ph/0511083)

Ivanov, V. D., Rieke, M. J., Engelbracht, C. W., Alonso-Herrero, A., Rieke, G. H., & Luhman, K. L. 2004, *ApJS*, 151, 387

Jeffries, R. D. & Tolley, A. J. 1998, *MNRAS*, 300, 331

Jeffries, R. D., Totten, E. J., & James, D. J. 2000, *MNRAS*, 316, 950

Jeffries, R. D., Oliveira, J. M., Barrado y Navascués, D., & Stauffer, J. R. 2003, *MNRAS*, 343, 1271

Jeffries, R. D., Naylor, T., Devey, C. R., Totten, E. J. 2004, *MNRAS*, 351, 1401

Jeffries, R. D. & Oliveira, J. M., 2005, *MNRAS*, 358, 13

Jeffries, R. D., Evans, P. A., Pye, J. P., & Briggs, K. R. 2006, *MNRAS*, 367, 781

Jura, M. 1990, *ApJ*, 365, 317

Kenyon, S. J. & Hartmann, L. 1995, *ApJS*, 101, 117

Kenyon, S. J. & Bromley, B. C. 2004a, *ApJ*, 602, L133

Kenyon, S. J. & Bromley, B. C. 2004b, *AJ*, 127, 513

Kenyon, S. J. & Bromley, B. C. 2005, *AJ*, 130, 269

Kenyon, S. J. & Bromley, B. C. 2006, *AJ*, 131, 1837

Kim, J. S., et al. 2005, *ApJ*, 632, 659

Kleine, T., Munker, C., Mezger, K., & Palme, H. 2002, *Nature*, 418, 952

Kleinmann, S. G. & Hall, D. N. B. 1986, *ApJS*, 62, 501

Kleinmann S. G., Cutri R. M., Young E. T., Low F. J., & Gillett F.C. 1986, IRAS Serendipitous Survey Catalog (On-line VizieR catalog II/126)

Lada, C. J. et al. 2006, *AJ*, 131, 1574

Littlefair, S. L., Naylor, T., Jeffries, R. D., Devey, C. R., & Vine, S. 2003, *MNRAS*, 345, 1205

Low, F. J., Smith, P. S., Werner, M., Chen, C., Krause, V., Jura, M., & Hines, D. C. 2005, *ApJ*, 631, 1170

Lyra, W., Moitinho, A., van der Blieck, N. S., & Alves, J. 2006, *A&A*, 453, 101

Mamejek, E. E., Meyer, M. R., Hinz, P. M., Hoffmann, W. F., Cohen, M., Hora, J. L. 2004, *ApJ*, 612, 496

Mathis, J. S. 1990, *ARA&A*, 28, 37

Megeath, S. T., Hartmann, L., Luhman, K. L., & Fazio, G. G. 2005, *ApJ*, L634, 113

Meixner, M. et al. 2006, *ApJ*, in press (astro-ph/0606356)

Meyer, M. R., Backman, D. E., Weinberger, A. J., & Wyatt, M. C. 2006, in "Protostars and Planets V", Univ. of Arizona Press, editors: B. Reipurth, D. Jewitt, and K. Keil

Meyer, M. R. et al. 2007, *PASP*, in press (astro-ph/0701058)

Moorwood, A., et al. 1998, *Messenger*, 94, 7

Moro-Martín, A. & Malhotra, R. 2002, *AJ*, 124, 2305

Munari, U. & Tomasella, L. 1999, *A&AS*, 137, 521

Naylor, T., Totten, E. J., Jeffries, R. D., Pozzo, M., Devey, C. R., & Thompson, S. A., 2002, *MNRAS*, 335, 291

Oliveira, J. M., Jeffries, R. D., Devey, C. R., Barrado y Navascués, D., Naylor, T., Stauffer, J. R., & Totten, E. J. 2003, *MNRAS*, 342, 651

Oudmaijer, R. D., Waters, L. B. F. M., van der Veen, W. E. C. J., & Geballe, T. R. 1995, *A&A*, 299, 69

Padgett, D. L. et al. 2006, *ApJ*, 645, 1283

Pascucci, I. et al. 2006, *ApJ*, 651, 1177

Patten, B. M., et al. 2006, *ApJ*, 651, 502

Plets, H., Waelkens, C., Oudmaijer, R. D., & Waters, L. B. F. M. 1997, *A&A*, 323, 513

Rhee, J. H., Song, I., & Zuckerman, B. 2007, *ApJ*, in press (astro-ph/0706.1265)

Riaz, B., Gizis, J. E., & Hmiel, A. 2006, *ApJ*, 639, L79

Rieke, G. H., et al. 2005, *ApJ*, 620, 1010

Robichon, N., Arenou, F., Mermilliod, J.-C., Turon, C. 1999, *A&A*, 345, 471

Schiavon, R. P., Barbuy, B., Rossi, S. C. F., & Milone, A. Sicilia-Aguilar, A. et al. 2006, *ApJ*, 638, 897

Sicilia-Aguilar, A. et al. 2007, *ApJ*, 659, 1637

Siegler, N., Muzerolle, J., Mamejek, E., Young, E., Rieke, G., Trilling, D., Gorlova, N., & Su, K. Y. L. 2006, *ApJ*, in press

Siess L., Dufour E., Forestini M. 2000, *A&A*, 358, 593

Silverstone, M. D., et al. 2006, *ApJ*, 639, 1138

Su, K. Y. L. et al. 2006, *ApJ*, submitted

Torres-Dodgen, A. V. & Weaver, W. B. 1993, *PASP*, 105, 693

Uzpen, B., et al. 2005, *ApJ*, 629, 512

Uzpen, B., et al. 2006, *ApJ*, in press (astro-ph/0612235)

Wallace, L. & Hinkle, K. 1997, *ApJS*, 111, 445

White, R. J. & Hillenbrand, L. A. 2005, *ApJ*, 621, L65

Worley C., E. & Douglass G., G. 1997, *A&AS*, 125, 523 (On-line VizieR catalog I/237)

Young, E. T., et al. 2004, *ApJS*, 154, 428

Zacharias N., Urban S. E., Zacharias M. I., Wycoff G. L., Hall D. M., Germain M. E., Holdenried E.R., & Winter L. 2003, The Second U.S. Naval Observatory CCD Astrograph Catalog

Zuckerman, B., Kim, S. S., & Liu, T. 1995, *ApJ*, 446, L79

TABLE 1  
*Spitzer* PHOTOMETRY FOR NGC 2547 HIGHLY-PROBABLE PHOTOMETRIC MEMBERS

RA ° (2000, 2MASS)	DEC °	V-K	R <sub>C</sub> -K	K <sup>1</sup>	±	[3.6]	±	[4.5]	±	[5.8]	±	[8.0]	±	[24]	±	Field No. <sup>2</sup>	Sta- No. <sup>3</sup>	
122.532396	-48.919441	99.99	1.17	11.62	0.02	11.61	0.00	11.63	0.01	11.66	0.02	11.56	0.03	99.99	99.99	23	2	
122.532740	-49.276600	-0.01	99.99	8.43	0.02	8.50	0.01	8.46	0.01	8.49	0.00	8.51	0.00	7.64 <sup>h</sup>	0.04	9	843	
122.534364	-49.183403	99.99	99.99	99.99	14.99	0.02	15.01	0.05	99.99	99.99	99.99	99.99	99.99	99.99	99.99	99.99	13	1770
122.534440	-49.332378	99.99	1.16	11.21	0.02	11.18	0.00	11.22	0.00	11.23	0.01	11.16	0.01	99.99	99.99	8	18	
122.535073	-49.012066	0.29	99.99	9.55	0.02	9.54	0.01	9.64	0.00	9.54	0.01	9.54	0.00	8.43	0.02	30	8420	
122.537235	-49.261490	3.28	2.58	12.19	0.03	12.06	0.00	12.13	0.01	12.06	0.03	12.03	0.08	99.99	99.99	13	174	
122.538460	-49.048122	99.99	2.17	12.27	0.03	12.24	0.01	12.34	0.01	12.22	0.02	12.25	0.04	99.99	99.99	18	103	
122.538682	-49.348309	1.64	1.27	10.81	0.02	10.82	0.00	10.82	0.00	10.88	0.01	10.81	0.01	10.74	0.16	8	19	
122.539099	-49.015720	2.06	99.99	10.43	0.02	10.42	0.00	10.59	0.00	10.37	0.01	10.36	0.01	10.35	0.11	18	42	
122.539829	-48.942863	99.99	2.54	12.22	0.03	12.14	0.00	12.23	0.01	12.21	0.02	12.14	0.04	99.99	99.99	18	110	
122.540051	-49.265015	2.89	2.24	11.20	0.02	11.13	0.00	11.20	0.00	11.11	0.01	10.97 <sup>c</sup>	0.03	10.57	0.14	13	114	
122.541465	-49.609333	99.99	2.67	11.33	0.03	11.21	0.00	11.42	0.00	11.31	0.01	11.28	0.02	99.99	99.99	3	32	
															PM? <sup>3</sup>			
122.532396	-48.919441														Y			
122.532740	-49.276600														Y			
122.534364	-49.183403														N/A			
122.534440	-49.332378														Y			
122.535073	-49.012066														Y			
122.537235	-49.261490														N			
122.538460	-49.048122														Y			
122.538682	-49.348309														Y			
122.539099	-49.015720														Y			
122.539829	-48.942863														Y			
122.540051	-49.265015														Y			
122.541465	-49.609333														Y			

## NOTE. —

Objects from this table are shown as solid circles on Figures 6, 7, 8, 9, 10, 11, except for those with questionable photometry (notes h, c). 99.99 means no data. The complete version of this table will be in the electronic edition of the ApJ. The printed edition contains only a sample.

<sup>1</sup> K<sub>S</sub> from 2MASS

<sup>2</sup> Designations from “Wide catalog” of Naylor et al. (2002) or from “RIZ” catalog of Jeffries et al. (2004)

<sup>3</sup> Proper motion membership flag (§3), N/A: proper motion not available

h Extended (halo-like) sources at 24  $\mu$ m

c Excess at 8  $\mu$ m may be due to contamination of the aperture by a nearby source, cosmic ray or strong nebulosity

TABLE 2  
*Spitzer* PHOTOMETRY FOR NGC 2547 LESS PLAUSIBLE PHOTOMETRIC MEMBERS

RA ° (2000, 2MASS)	DEC °	V-K	R <sub>C</sub> -K	K	±	[3.6]	±	[4.5]	±	[5.8]	±	[8.0]	±	[24]	±	Field No.	Star No.
122.716280	-48.971233	2.84	99.99	11.06	0.02	11.02	0.00	11.14	0.00	11.08	0.01	10.98	0.01	99.99	99.99	18	490
122.730125	-49.443478	4.84	99.99	13.80	0.04	13.53	0.01	13.47	0.01	13.42	0.06	13.45	0.08	99.99	99.99	9	1394
122.747649	-49.142479	5.12	99.99	13.50	0.04	13.23	0.01	13.19	0.01	13.19	0.06	13.18	0.08	99.99	99.99	12	1176
122.769807	-49.054371	3.96	99.99	11.85	0.04	11.73	0.01	11.64	0.01	11.60	0.02	11.64	0.04	99.99	99.99	19	1086
122.802249	-49.093540	5.60	99.99	14.43	0.07	14.12	0.04	14.09	0.04	13.72	0.11	13.41 <sup>c</sup>	0.10	99.99	99.99	19	633
122.803718	-49.162022	2.50	99.99	10.85	0.02	10.80	0.00	10.89	0.00	10.84	0.01	10.81	0.01	99.99	99.99	12	137
122.819776	-49.115688	99.99	4.02	14.80	0.10	14.47	0.02	14.36	0.03	14.22	0.10	13.94	0.14	99.99	99.99	12	731 <sup>nm</sup>
122.836424	-49.219448	1.35	99.99	10.69	0.02	10.68	0.00	10.66	0.00	10.71	0.01	10.66	0.01	99.99	99.99	12	22
122.836981	-49.151585	1.68	99.99	11.39	0.02	11.31	0.00	11.39	0.01	11.36	0.02	11.29	0.02	99.99	99.99	12	64
122.899746	-48.946228	3.17	99.99	10.95	0.02	10.90	0.00	11.00	0.00	10.96	0.01	10.88	0.01	99.99	99.99	19	910
122.910886	-49.239845	5.29	99.99	13.87	0.05	13.70	0.01	13.69	0.02	13.58	0.06	13.68	0.09	99.99	99.99	12	2353
122.945855	-49.215736	3.55	99.99	12.06	0.02	11.96	0.00	12.05	0.01	11.94	0.02	12.00	0.03	99.99	99.99	12	1013
														PM? <sup>3</sup>			
122.716280	-48.971233													Y			
122.730125	-49.443478													N/A			
122.747649	-49.142479													N/A			
122.769807	-49.054371													N			
122.802249	-49.093540													N/A			
122.803718	-49.162022													N			
122.819776	-49.115688													N/A			
122.836424	-49.219448													Y			
122.836981	-49.151585													N			
122.899746	-48.946228													Y			
122.910886	-49.239845													N/A			
122.945855	-49.215736													N			

NOTE. —  
Objects from this table are shown as triangles on Fig. 6, 8, 10, except for those with notes.  
For description of columns see Table 1. The complete version of this table will be in the electronic edition of the ApJ. The printed edition contains only a sample.

ns Non-stellar flag in Jeffries et al. (2004)

nm Below the cluster sequence on the V - (V - K) or R - (R - K) diagram - nonmember?

<sup>c</sup> Excess at 8  $\mu$ m may be due to contamination of the aperture by a nearby source

TABLE 3  
LOG OF IMACS OBSERVATIONS

Mask No.	Mask Center		UT Date	Airmass	Seeing FWHM(")	Integr. Time sec × frames	V mag
	RA (h:min:s)	DEC ( $^{\circ} : ' : ''$ )					
1	08:09:40.000	-49:12:00.00	2005 Feb 02	1.11–1.12	0.6	15 × 7	9-13
2	08:09:40.000	-49:12:00.00	2005 Dec 23	1.07–1.11	0.6	900 × 3	13-19
3	08:10:36.000	-49:15:00.00	2005 Dec 21	1.09–1.10	0.6	150 × 3	10-12
4	08:10:36.000	-49:15:00.00	2005 Feb 03	1.13–1.18	0.7	600 × 3	13-15
5	08:09:40.000	-48:57:30.00	2005 Dec 21	1.07–1.07	0.6	900 × 3	13-18

TABLE 4  
IMACS SPECTROSCOPY OF NGC 2547 CANDIDATE MEMBERS

2MASS	$(V - K)_0$	$V_0$	$(K - [8])_0$	$(K - [24])_0$	SpT <sup>1</sup>	RV <sup>2</sup> group	Prob. <sup>3</sup> %	RV <sup>4</sup> km/s	S/N <sup>5</sup>	Sp. No <sup>6</sup> mask:slit	Remarks <sup>7</sup>
08095753-4908202	-0.20	8.73	0.05	1.62	A0Vn	BF	37	67	83	1:23	Broad lines
08093671-4911383	0.02	8.67	-0.05	-0.05	A0-A1	BF	52	59	280	1:19	Broad lines
08100607-4914180	0.04	9.68	0.02	1.47	B8-A1	BF	59	32	38	1:18	Low S/N
08095221-4911022	0.06	9.48	99.99	99.99	BF	54	34	120	1:7	Broad lines	
08092958-4906166	0.35	10.03	99.99	99.99	A0-A2V	BF	48	19	180	1:22	Broad lines
08095066-4912493	0.36	10.03	-0.05	0.02	A2-A3IV	BF	66	18	93	1:21	
08095060-4913194	0.53	10.40	99.99	99.99	A0	G	0	12	95	3:7	Broad lines
08094610-4914270	0.53	10.49	-0.00	-0.00	F0	BF	99.99	20	79	1:13	
08092668-4914371	0.58	10.70	0.04	1.27	99.99	BF	51	11	120	1:8	
08093053-4920443	0.81	10.90	0.01	0.07	F0	BF	52	13	104	1:14	Broad lines
08091401-4904029	0.84	11.23	0.14	0.16	99.99	G	65	1	91	1:17	Broad lines; ID 1
08104662-4917312	0.89	10.57	0.01	0.11	99.99	G	34	-5	31	3:5	Low S/N
08094893-4909370	0.93	10.74	99.99	99.99	BF	4	10	79	1:11	Broad lines	
08093815-4918403	0.96	10.62	0.11	0.95	A7-A9	BF	42	16	110	1:20a	ID 2a
08093815-4918403	0.96	10.62	0.11	0.95	99.99	K	42	39	72	1:20b	ID 2b
08090287-4906022	1.02	11.60	0.02	-0.07	99.99	G	51	0.6	56	1:26	
08100087-4908324	1.04	10.80	-0.01	0.01	99.99	BF	44	13	31	1:9	Emission? Low S/N
08101352-4920438	1.10	10.78	0.00	0.03	99.99	BF	22	26	15	1:10	Low S/N
08092293-4907575	1.14	12.00	-0.06	0.60	99.99	K	26	9	81	1:15	
08102774-4912095	1.15	10.81	0.04	-0.14	99.99	G	19	-10.6	46	3:6	
08104984-4911258	1.16	11.58	0.06	0.14	99.99	G	29	6	29	3:8	
08112074-4913100	1.18	11.85	0.02	99.99	99.99	G	46	19	20	3:10	
08103470-4908399	1.30	12.20	-0.03	0.05	99.99	G	13	5	27	3:9	
08095109-4859022	1.37	12.96	0.10	99.99	99.99	G	0	49	99	5:23	
08085790-4854189	1.38	99.99	0.02	99.99	99.99	G	99.99	14	97	5:28	
08100380-4901071	1.49	12.36	0.02	0.02	99.99	G	42	8	120	5:14	Broad lines
08093456-4920553	1.58	13.01	0.03	0.87	99.99	K	40	27	190	2:13	
08090250-4858172	1.61	12.95	1.54	3.66	99.99	G	99.99	14	62	5:11	ID 8
08095421-4919220	1.62	12.50	0.01	-0.09	99.99	K	99.99	16	29	1:27	
08094117-4855146	1.63	99.99	0.03	99.99	99.99	G	99.99	22	84	5:32	
08110234-4916249	1.65	12.90	0.01	0.79	99.99	K	64	16	35	4:8	
08101542-4911095	1.81	13.03	0.18	99.99	99.99	K	49	70	29	4:6	
08103793-4914225	1.87	13.20	0.11	99.99	99.99	K	57	17	36	4:9	
08092276-4916309	1.91	13.42	0.07	99.99	99.99	K	7	7	170	2:14	Emission
08101292-4914094	1.92	13.45	0.02	99.99	99.99	K	99.99	13	190	2:9	Emission
08095274-4922170	1.97	13.33	-0.06	99.99	99.99	K	0	26	160	2:15	
08101799-4923502	2.09	13.71	0.05	99.99	99.99	K	41	14	22	4:11	Low S/N
08091928-4904260	2.19	14.26	0.15	99.99	K3e	K	99.99	21	26	5:36	
08110637-4912267	2.19	13.97	0.08	99.99	99.99	K	36	23	22	4:13	
08092916-4901240	2.20	14.17	0.01	99.99	99.99	K	6	3	29	5:10	
08091332-4857599	2.20	13.72	0.14	99.99	99.99	K	99.99	0	40	5:33	Emission?
08092129-4900412	2.20	14.13	0.05	99.99	99.99	K	59	1	38	5:35	
08085572-4857167	2.41	14.49	0.14	99.99	99.99	K	99.99	31	31	5:17	
08104410-4913153	2.41	13.33	0.06	99.99	99.99	K	71	68	37	4:7	
08101944-4907444	2.42	14.02	0.09	99.99	99.99	K	66	-30	170	2:17	
08092387-4915041	2.50	13.94	0.01	99.99	99.99	K	0	22	130	2:24	
08101474-4912320	2.51	13.39	0.12	0.74	99.99	K	3	110	220	2:7	
08090022-4920332	2.56	14.41	0.03	99.99	99.99	K	40	9	110	2:20	Emission
08100398-4913027	2.65	13.87	0.14	99.99	99.99	K	99.99	4	140	2:10a	
08094482-4902195	2.67	14.15	0.06	99.99	99.99	K	99.99	54	40	5:29	
08100961-4915540	2.72	13.90	0.22	0.61	99.99	K	48	8	170	2:8	
08101083-4858477	2.74	14.41	0.06	99.99	99.99	K	38	73	52	5:8	
08101987-4856000	2.75	14.46	0.05	99.99	99.99	K	99.99	16	66	5:24	Emission
08100558-4914581	2.77	14.46	0.21	99.99	99.99	K	26	35	140	2:11	
08091164-4857019	2.77	14.87	0.12	99.99	99.99	K	99.99	70	24	5:20	
08092019-4907045	2.79	14.41	0.11	99.99	99.99	K	0	33	150	2:16	
08101679-4913171	2.84	14.76	-0.01	99.99	99.99	K	0	91	110	2:18	
08092683-4900187	2.94	14.73	0.10	99.99	99.99	K	0	50	30	5:19	
08101691-4856291	3.10	14.20	3.10	6.99	99.99	K	99.99	29	64	5:12	Broad lines; ID 9
08100955-4856343	3.11	15.31	0.06	99.99	99.99	K	99.99	68	47	5:21	
08100893-4915413	3.12	15.29	0.15	99.99	K7e	K	0	-13	15	4:17	Low S/N; emiss.?
08100442-4850544	3.21	99.99	0.06	99.99	99.99	K	99.99	26	17	5:38	
08103186-4921296	3.25	15.04	0.14	99.99	K7e	K	62	-14	17	4:12	Low S/N; emiss.?
08100759-4900035	3.27	14.44	0.18	0.47	99.99	K	69	136	49	5:25	
08095507-4858140	3.57	15.96	0.16	99.99	99.99	K	99.99	15	23	5:22	Emission
08102318-4912086	3.61	15.99	0.20	99.99	99.99	M	99.99	17	90	2:26	Emission
08091657-4909309	3.62	15.92	0.26	99.99	M0e	M	99.99	11	84	2:21	Emission
08100749-4910447	3.72	16.09	0.07	99.99	M0e	M	99.99	16	92	2:23	Emission
08091025-4902250	3.74	15.85	0.38	0.27	99.99	M	0	10	18	5:18	Emission
08093105-4853166	3.75	99.99	0.04	99.99	99.99	K	99.99	89	28	5:27	
08094556-4917364	3.90	16.12	0.16	99.99	M0e	M	99.99	9	68	2:19	Low S/N
08102553-4906335	3.98	16.56	0.18	99.99	M1e	M	99.99	16	80	2:28	Emission
08093685-4914214	4.00	15.74	0.27	99.99	M1e	M	99.99	17	100	2:12	Emission
08102150-4901339	4.21	17.03	0.21	99.99	99.99	M	99.99	10	27	5:30	Low S/N; emiss.?

TABLE 4 — *Continued*

2MASS	$(V - K)_0$	$V_0$	$(K - [8])_0$	$(K - [24])_0$	SpT <sup>1</sup>	RV <sup>2</sup> group	Prob. <sup>3</sup> %	RV <sup>4</sup> km/s	S/N <sup>5</sup>	Sp. No <sup>6</sup> mask:slit	Remarks <sup>7</sup>
08092437-4906282	4.27	17.04	0.19	99.99	M2e	M	99.99	8	68	2:31	Emission
08092131-4905540	4.36	16.64	0.25	99.99	99.99	M	99.99	13	86	2:25	Emission
08100180-4915454	4.42	17.38	0.19	99.99	M1e	M	99.99	12	61	2:29	Emission
08102210-4911230	4.43	17.47	0.42	99.99	M2e	M	99.99	22	64	2:32	Emission
08102103-4910448	4.64	17.81	0.08	99.99	M3e	M	99.99	17	58	2:33	Emission
08093892-4915051	4.70	17.34	0.19	99.99	99.99	M	99.99	16	61	2:22	Emission
08095429-4908418	4.71	18.27	0.21	99.99	99.99	M	99.99	15	48	2:37	Emission
08085758-4911261	4.77	18.16	0.15	99.99	99.99	M	99.99	12	42	2:34	Emission
08094273-4921168	4.85	18.64	0.22	99.99	99.99	M	99.99	11	34	2:38	
08091111-4914183	5.03	18.19	0.39	99.99	99.99	M	99.99	6	361	2:30	
08094499-4906241	5.06	18.04	0.72	99.99	M4e	M	99.99	15	48	2:35	
08092592-4909585	5.07	18.45	0.03	99.99	99.99	M	99.99	8	43	2:36	Emission ?
08100063-4853392	5.24	99.99	0.12	99.99	99.99	M	99.99	8	16	5:31	
08094946-4916189	5.49	18.59	0.36	99.99	99.99	M	99.99	17	47	2:27	
08093547-4913033	5.50	19.55	0.95	3.70	M4.5	M	99.99	11	28	2:6	ID 7

NOTE. — Magnitudes de-reddened assuming uniform reddening of  $A_V = 0.19$ . Where  $V$  is unavailable, we estimated  $V - K$  from  $I - K$  vs  $V - K$  sequence constructed for cluster members. Objects sorted according to  $(V - K)_0$ . Radial velocities and spectra are not reliable when S/N is low or lines are broad.

<sup>1</sup> Range of spectral types found in the *VizieR*

<sup>2</sup> Rough estimate of the spectral type for use with the corresponding radial velocity template, a combination of the actual SpT and the airmass of observation (see §3.2)

<sup>3</sup> Membership probability based on proper motion from Dias et al. (2006)

<sup>4</sup> Heliocentric velocity (as explained in §3.2)

<sup>5</sup> Signal-to-noise of spectrum estimated as the square root of counts in the continuum near 8490Å

<sup>6</sup> Designation of spectrum based on the mask number (Table 3) and slit number within the mask

<sup>7</sup> ID for stars with 8  $\mu$ m excess, their spectra shown on Fig. 4. Emission means emission inside Ca II NIR absorption lines

TABLE 5  
 NGC 2547 MEMBERS WITH MID-IR EXCESS

2MASS Name	Sp. No	$(V - K)_0$	$(R - K)_0$	$(K - [8])_0^1$	$(K - [24])_0^1$	Remarks <sup>2</sup>
Selected based on 8 $\mu\text{m}$ excess:						
08091401-4904029	1:17	0.84	99.99	<b>0.14</b>	0.16	ID 1
08093815-4918403	1:20a, 1:20b	0.96	99.99	<b>0.11</b>	<b>0.95</b>	ID 2; EXC $K$ , [3]
08090720-4919144	99.99	2.76	2.04	<b>0.26</b>	99.99	ID 4; EXC [4], [5]
08093547-4913033	2:6	5.50	4.29	<b>0.95</b>	<b>3.70</b>	ID 7; EXC [5]
08090250-4858172	5:11	1.61	1.25	<b>1.55</b>	<b>3.66</b>	ID 8; EXC [3], [4], [5]
08101691-4856291	5:12	3.10	2.47	<b>3.10</b>	<b>6.99</b>	ID 9; EXC $K$ , [3], [4], [5]
Selected based on 24 $\mu\text{m}$ excess:						
08092602-4911553	99.99	-0.18	99.99	0.04	<b>0.22</b>	
08084981-4913437	99.99	-0.04	99.99	0.02	<b>0.17</b>	
08100607-4914180	1:18	0.04	99.99	0.02	<b>1.47</b>	
08112585-4912288	99.99	0.08	99.99	-0.01	<b>0.70</b>	
08104233-4857253	99.99	0.12	99.99	0.00	<b>0.28</b>	
08100841-4900434	99.99	0.12	99.99	0.00	<b>1.10</b>	
08110323-4900374	99.99	0.57	99.99	0.03	<b>1.08</b>	
08092668-4914371	1:8	0.58	99.99	0.04	<b>1.27</b>	
08084571-4923473	99.99	0.62	99.99	0.00	<b>0.96</b>	
08111134-4904442	99.99	0.71	99.99	0.07	<b>0.54</b>	
08101673-4915173	99.99	0.72	99.99	0.03	<b>0.79</b>	
08092293-4907575	1:15	1.14	99.99	-0.06	<b>0.60</b>	
08104546-4901068	99.99	1.23	99.99	0.05	<b>0.43</b>	
08101836-4906461	99.99	1.27	99.99	0.01	<b>0.42</b>	
08094507-4856307	99.99	1.27	99.99	-0.01	<b>0.45</b>	
08085576-4923085	99.99	1.33	99.99	0.00	<b>0.36</b>	
08090344-4859210	99.99	5.37	99.99	0.60	<b>4.62</b>	
Selected based on possible 24 $\mu\text{m}$ excess:						
08104815-4923385	99.99	1.51	1.15	-0.01	<b>0.62</b>	
08093456-4920553	2:13	1.59	1.20	0.03	<b>0.87</b>	
08110009-4906442	99.99	1.59	1.23	0.03	<b>0.84</b>	
08110234-4916249	4:8	1.65	1.24	0.01	<b>0.79</b>	
08101474-4912320	2:7	2.51	99.99	0.12	<b>0.74</b>	RV & PM NM
08100961-4915540	2:8	2.72	2.12	0.22	<b>0.61</b>	
08091758-4859252	99.99	2.67	2.11	0.09	<b>0.69</b>	
08125256-4912123	99.99	99.99	2.21	99.99	<b>1.48</b>	
08102491-4851482	99.99	99.99	1.83	0.12	<b>1.90</b>	PM NM
08091770-4908344	99.99	5.56	4.30	0.64	<b>3.18</b>	

<sup>1</sup> In bold are colors indicating excess

<sup>2</sup> RV: radial velocity; PM: proper motion; NM: non-member; EXC: “excess also at”, square brackets denote IRAC wavebands in  $\mu\text{m}$

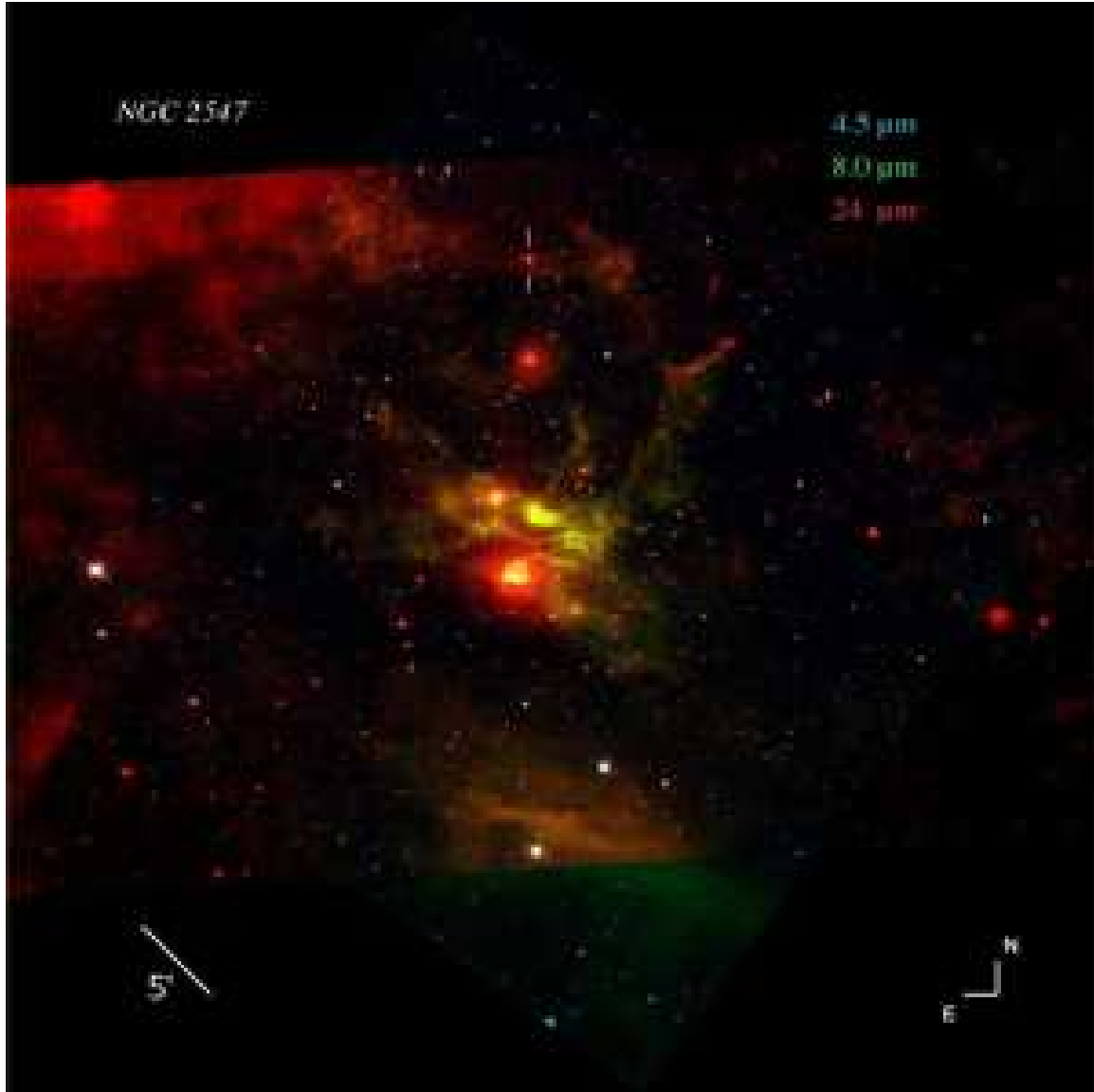


FIG. 1.— NGC 2547 color mosaic composed of two IRAC bands and the MIPS 24  $\mu\text{m}$  one. The optically brightest members in the center of the cluster are surrounded by extended 24  $\mu\text{m}$  emission, a result of winds and heating of the interstellar cirrus. They also excite the 7.7  $\mu\text{m}$  aromatic feature, seen as the bright green area. Two dashes indicate position of ID 9, a candidate low-mass member with a strong mid-IR excess.

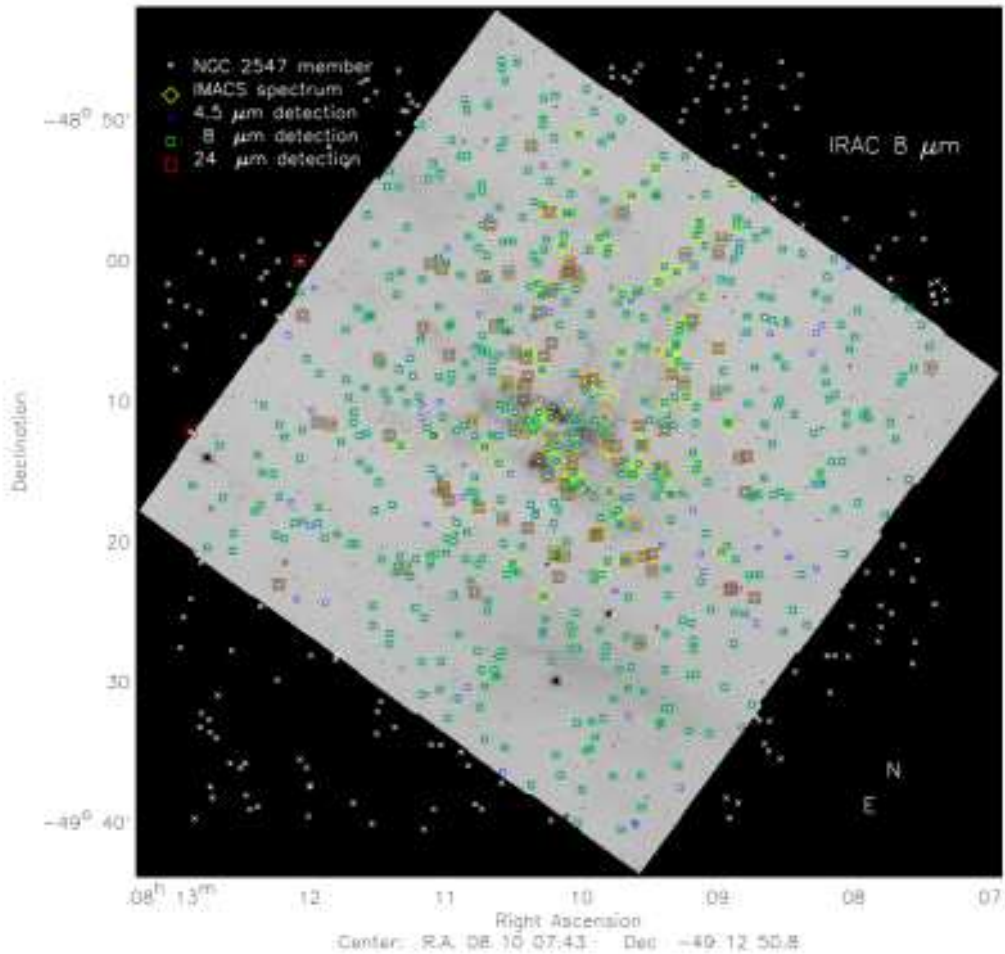


FIG. 2.— IRAC 8  $\mu\text{m}$  image showing area surveyed photometrically and spectroscopically in this work. Asterisks: optically-selected photometric members from Naylor et al. (2002) and Jeffries et al. (2004); squares: members detected with *Spitzer*, diamonds: sources for which we obtained spectra.

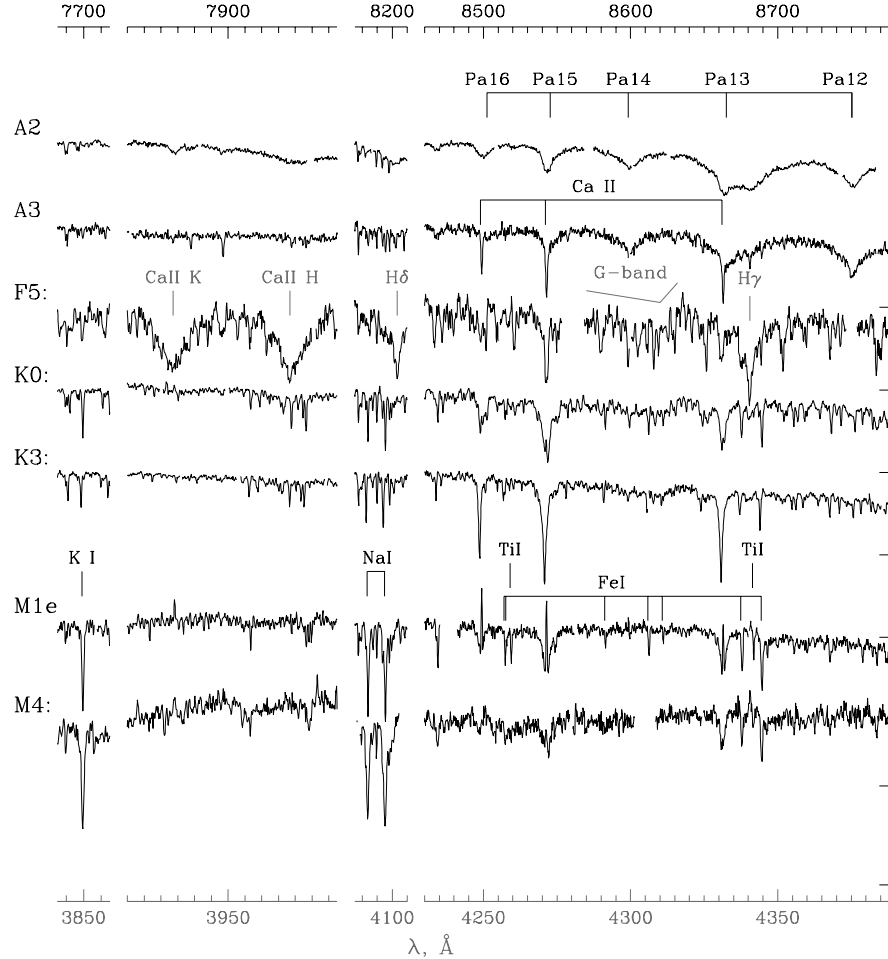


FIG. 3.— Spectroscopic sequence in NGC 2547 based on the representative IMACS spectra of non-excess stars. All spectral segments have been normalized to unity at the short-wavelength end and shifted vertically for clarity; horizontal dashes on the right mark the level of the zero flux for each spectrum. Spectral features marked in *black* with the wavelength scale given at top correspond to the red light (flux transmitted in the 1-st grating order). Features marked in *grey* with the wavelength scale on bottom correspond to the blue light (unblocked flux from the 2-nd order). The wavelength scale is heliocentric. Line identifications are from Munari & Tomasella (1999), Torres-Dodgen & Weaver (1993), and the Digital Spectral Classification Atlas of R. O. Gray. Examples of fast and slow rotation are given for A types, and with and without emission in the Ca II lines for K and M types. Colon means that spectral type was estimated based on the  $V - K$  color. From top to bottom: 2MASS08092958-4906166, 2MASS08095066-4912493, 2MASS08102774-4912095, 2MASS08101292-4914094, 2MASS08101944-4907444, 2MASS08093685-4914214, 2MASS08092592-4909585.

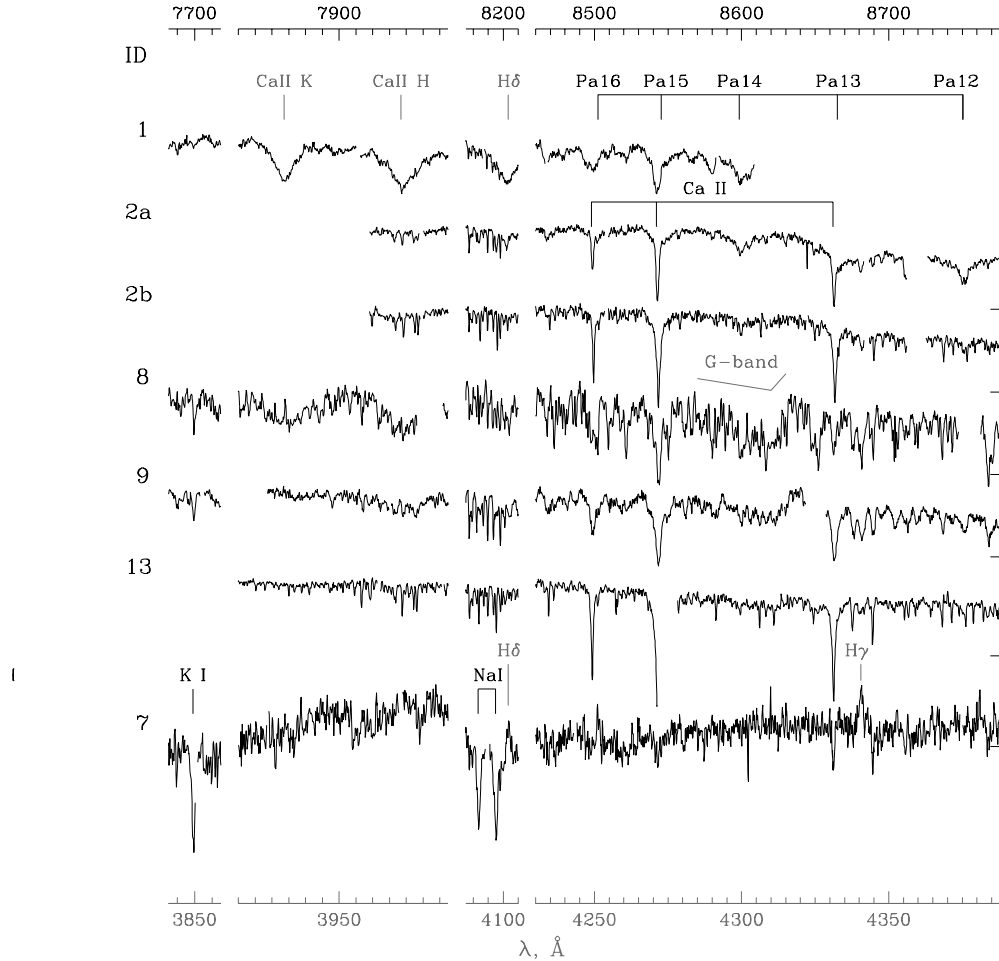


FIG. 4.— IMACS spectra of some excess stars from Table 5. From top to bottom: 2MASS08091401-4904029, 2MASS08093815-4918403 (resolved into two components), 2MASS08090250-4858172, 2MASS08101691-4856291, 2MASS08100961-4915540, 2MASS08093547-4913033. They compare well with spectra of non-excess members in Fig. 3.

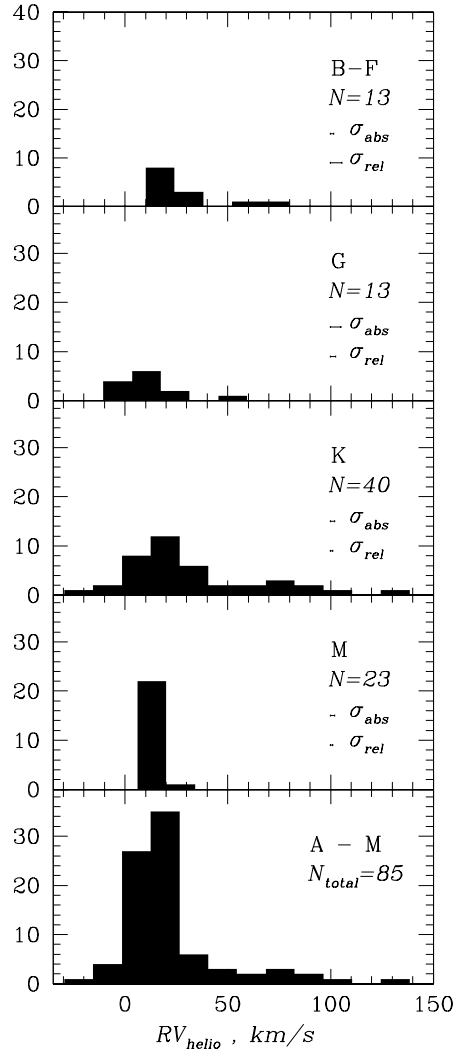


FIG. 5.— Distribution of radial velocities in NGC 2547 measured from IMACS spectra relative to the respective template in each spectral group. Contamination of K type members by background giants can be seen from the secondary peak at  $75 km/s$ .  $N$  gives the number of spectra in each group.

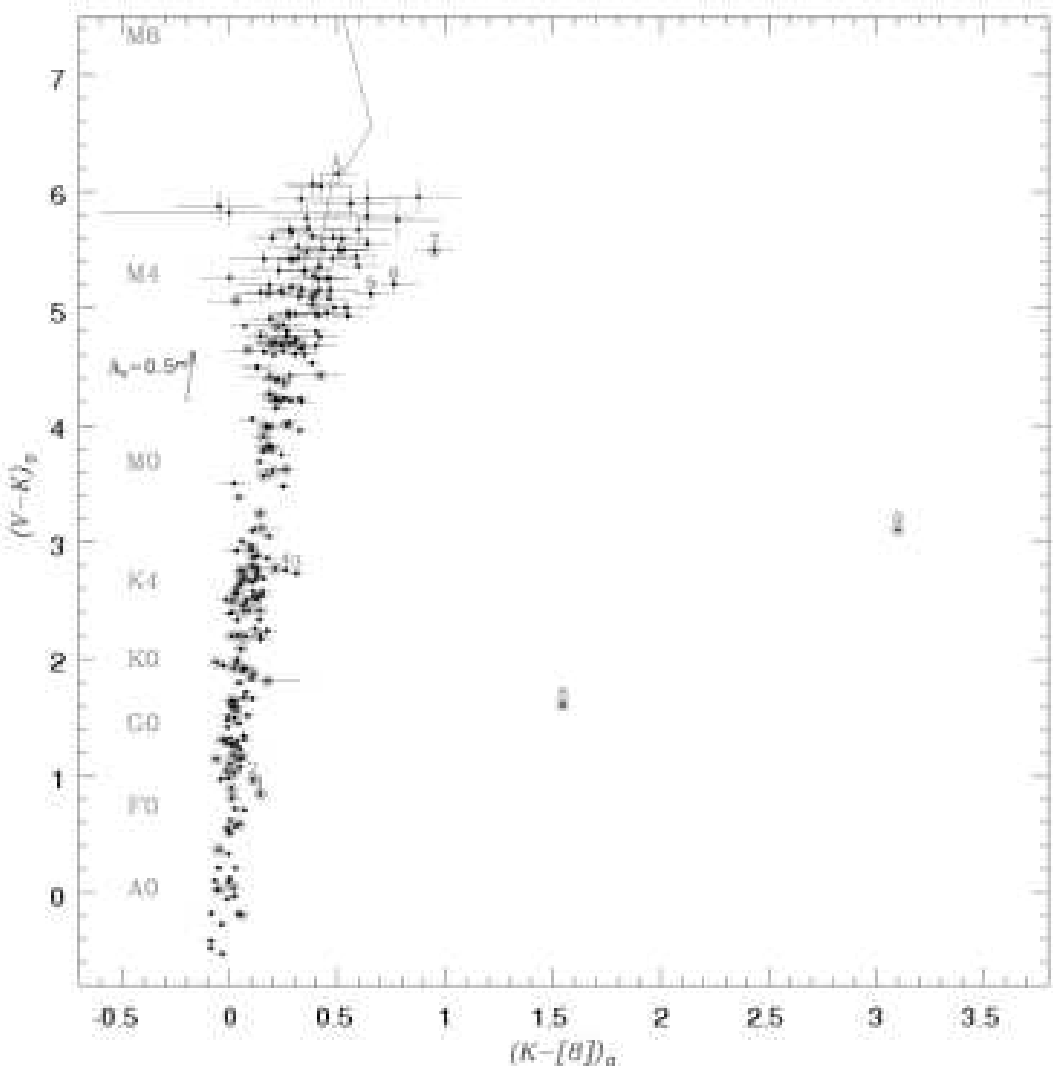


FIG. 6.— Color-color diagram (de-reddened) for identifying  $8 \mu\text{m}$  excesses using  $V - K$  color to trace photospheric flux. *Solid circles*:  $BVRIZ$ -selected NGC 2547 members (from Table 1); *triangles*:  $BV$ -selected possible members (from Table 2); *open circles*: spectroscopically observed (from Table 4). The solid line connects seven M3–M6.5 field dwarfs from Patten et al. (2006),  $V$  mags are taken from VizieR.

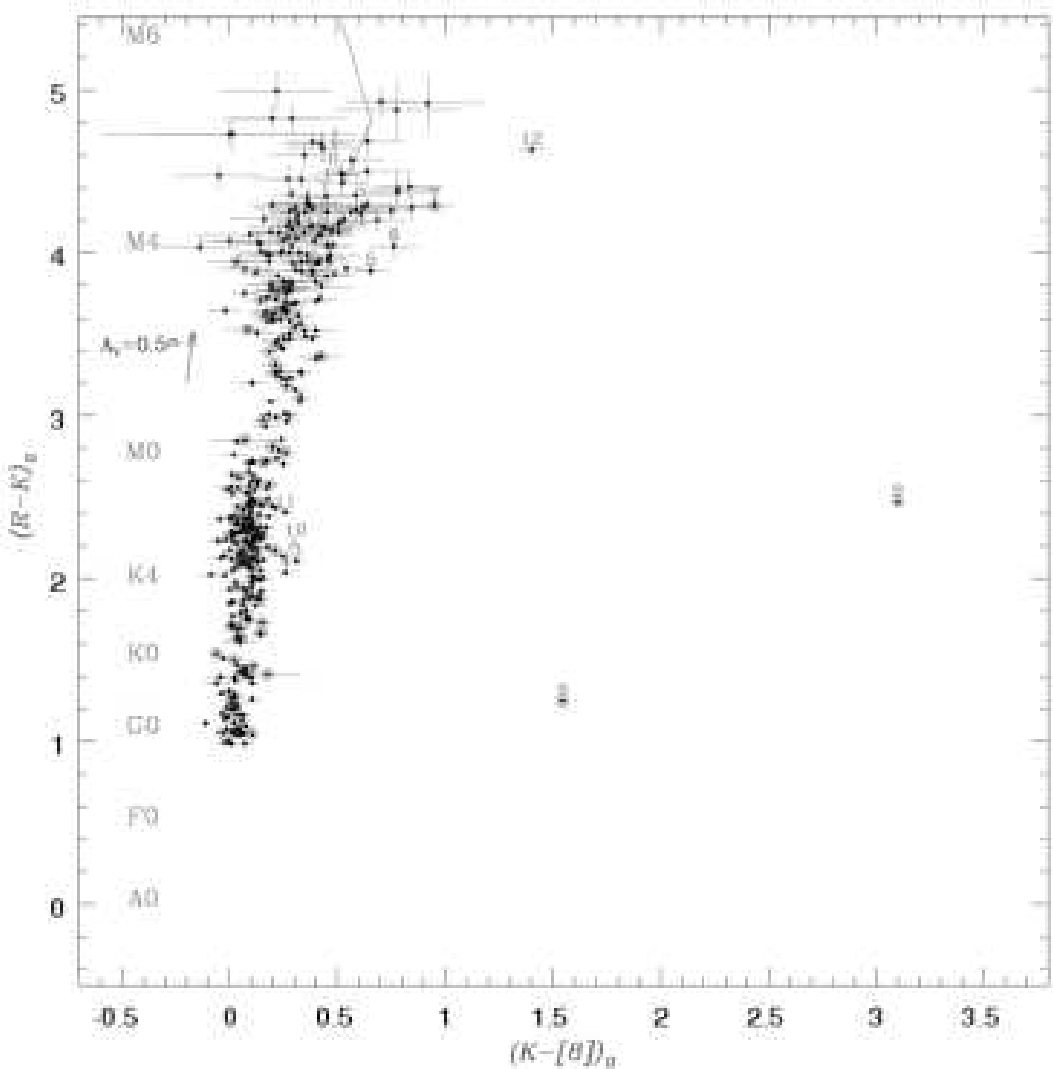


FIG. 7.— Color-color diagram for identifying 8  $\mu\text{m}$  excesses using  $R - K$  color to trace photospheric flux. Symbols same as in Fig. 6.  $R$  mags for field dwarfs of Patten et al. (2006) are derived from  $V - R$  vs. SpT relation of Kenyon & Hartmann (1995).

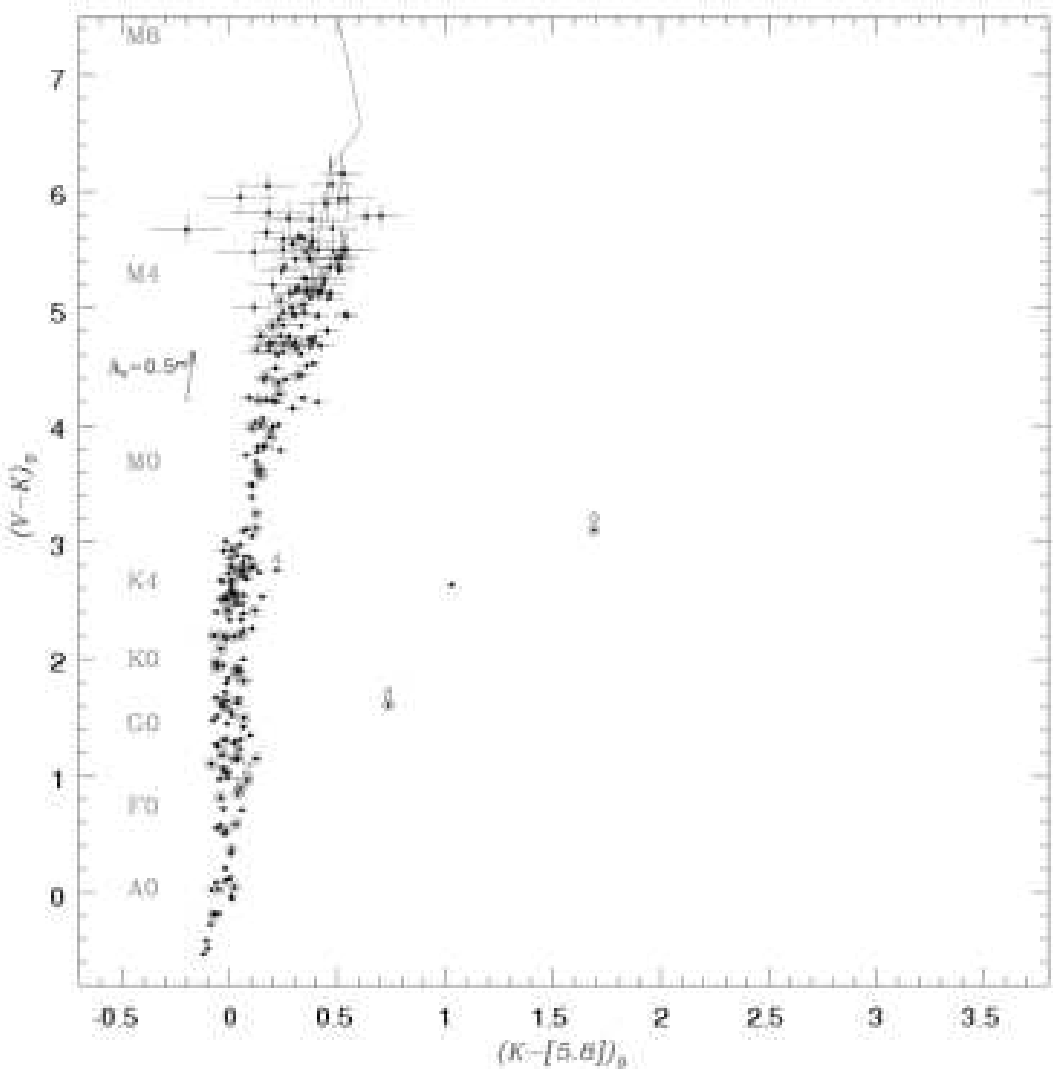


FIG. 8.— Color-color diagram to confirm  $8 \mu\text{m}$  excesses in the neighboring  $5.8 \mu\text{m}$  IRAC band. Symbols same as in Fig. 6.

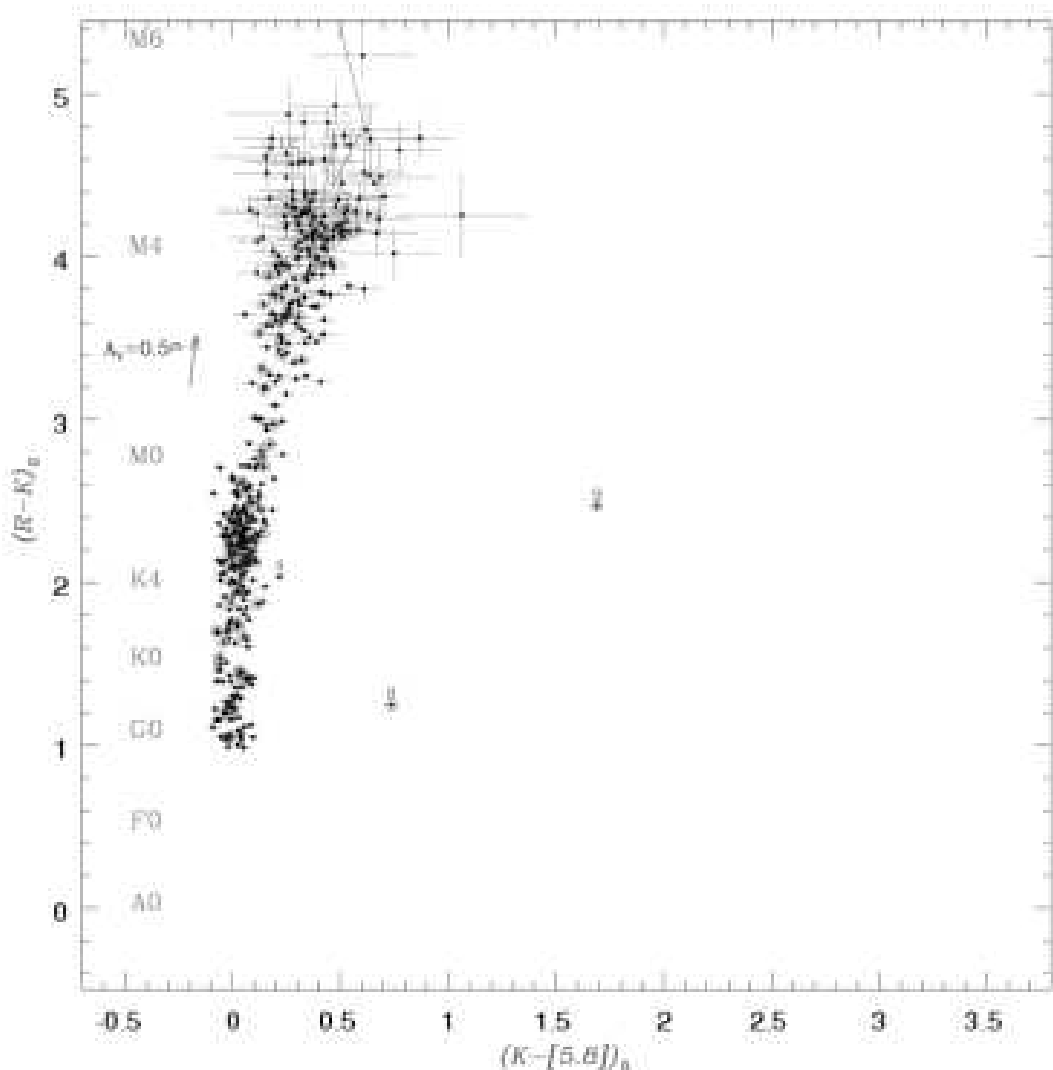


FIG. 9.— Similar diagram as in Fig. 8 but with  $R - K$  color.

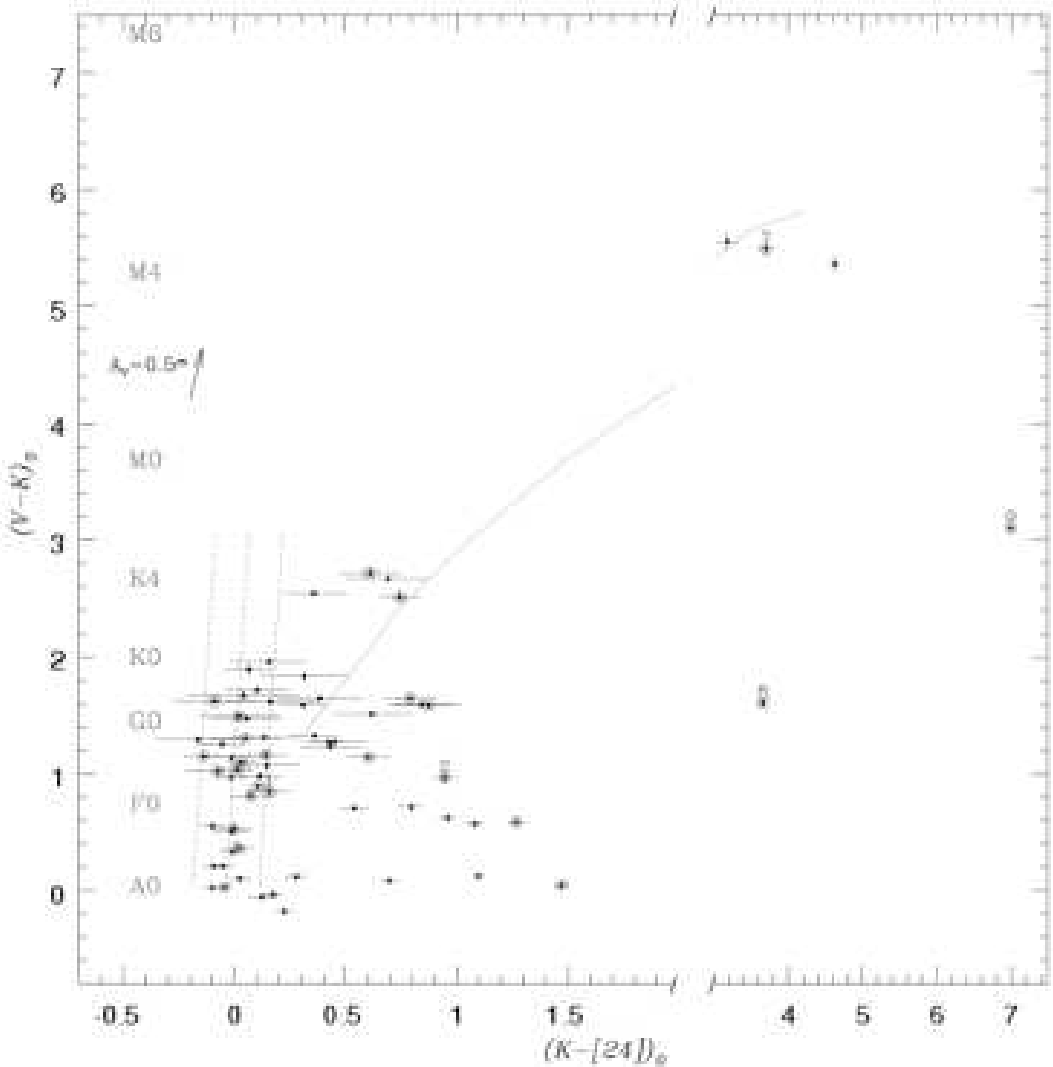


FIG. 10.— Color-color diagram used to identify 24  $\mu\text{m}$  excesses. The solid gray line represents our detection limit at 24  $\mu\text{m}$ . It approximates the locus of the non-detected members by assuming their  $[24] < 10.8^m$ , and so is a reflection of the  $K$  vs  $V - K$  sequence. It shows that we are complete at 24  $\mu\text{m}$  up to  $V - K \sim 1.3$  (late Fs). Objects to the left of this line are either binaries or situated in the very clean from nebulosity region. Dashed lines are the non-excess locus  $\pm 3 \sigma$  derived for the Pleiades stars (from Gorlova et al. (2006)), which we utilize here to identify excesses in NGC 2547. Symbols are the same as on the previous figures. The triangle at (4.62, 5.37) is 2MASS08090344-4859210 discussed in §5.1.

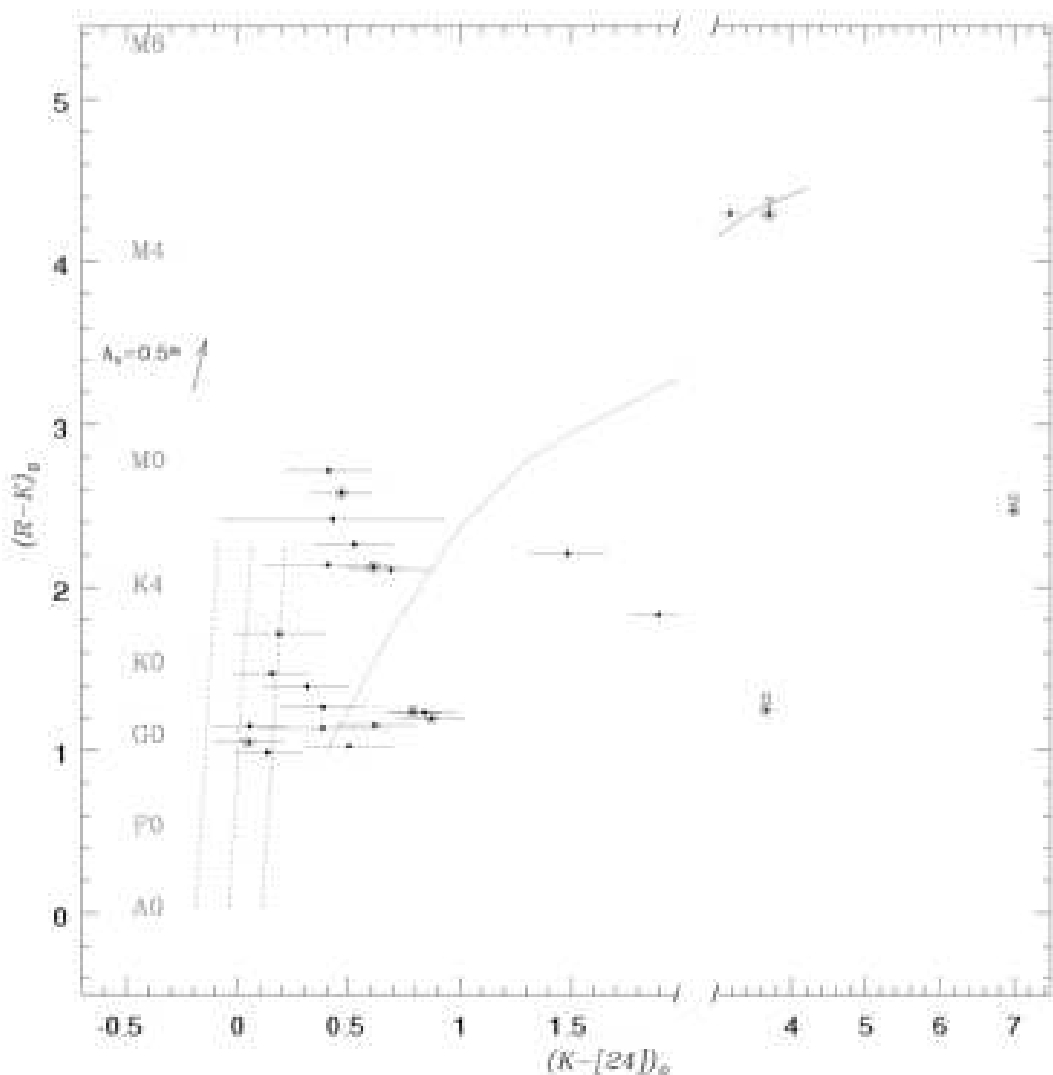


FIG. 11.— Same diagram as in Fig. 10 but with  $R - K$  color.

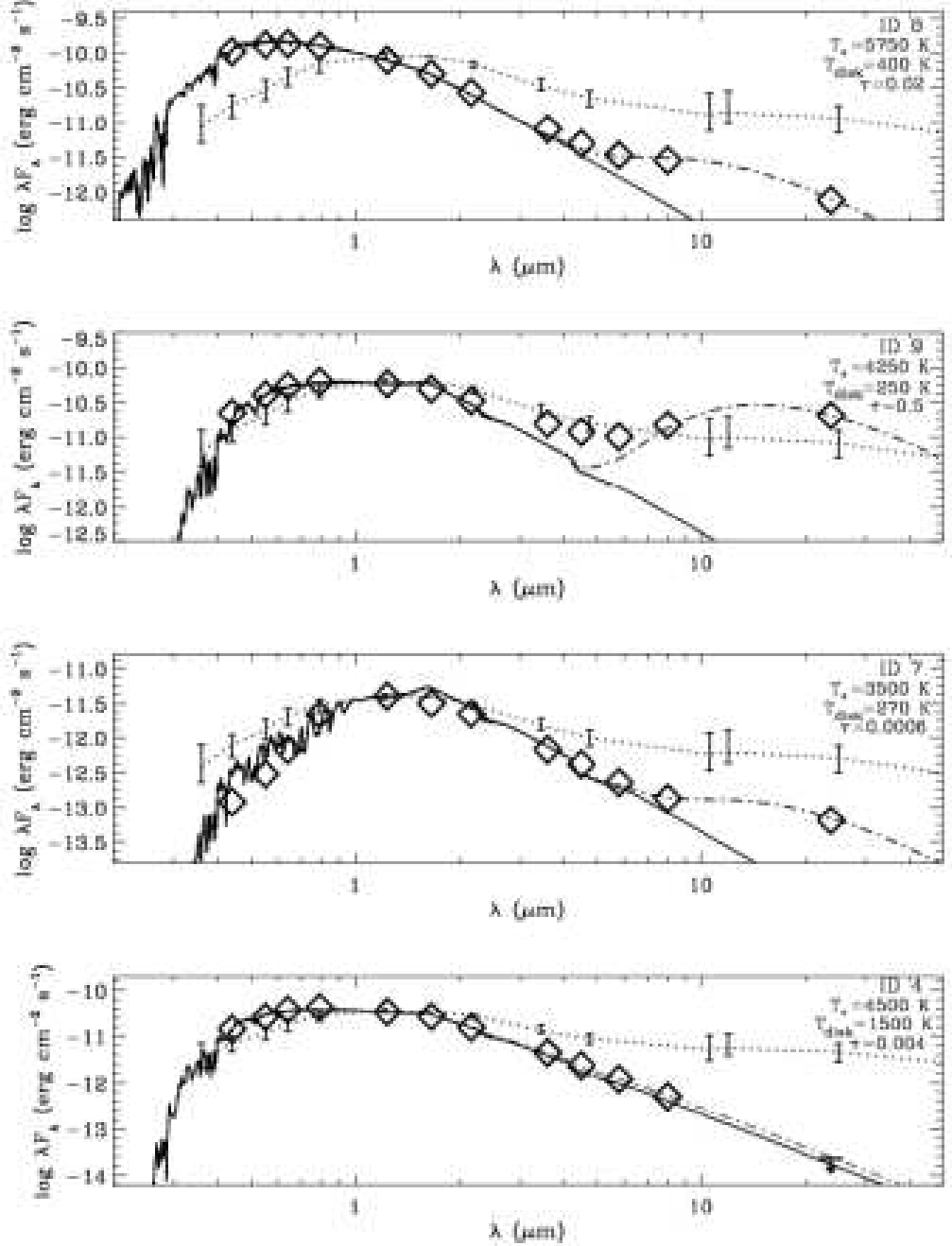


FIG. 12.—Spectral energy distributions of stars with 8  $\mu\text{m}$  excess. Diamonds:  $\text{BVR}I\text{JHK}$ , IRAC and MIPS 24  $\mu\text{m}$  derddened photometry ( $A_V = 0.19$ , extinction coefficients from Mathis (1990)); solid line: Kurucz photospheric model spectra with effective temperature  $T_*$  and  $\log g = 3.0$ ; dot-dashed line: photospheric flux plus a black-body flux of temperature  $T_{disk}$  and fractional luminosity  $\tau$ ; dotted line: median SED with the quartiles of the distribution for the class II K7–M2 sources in the Taurus.

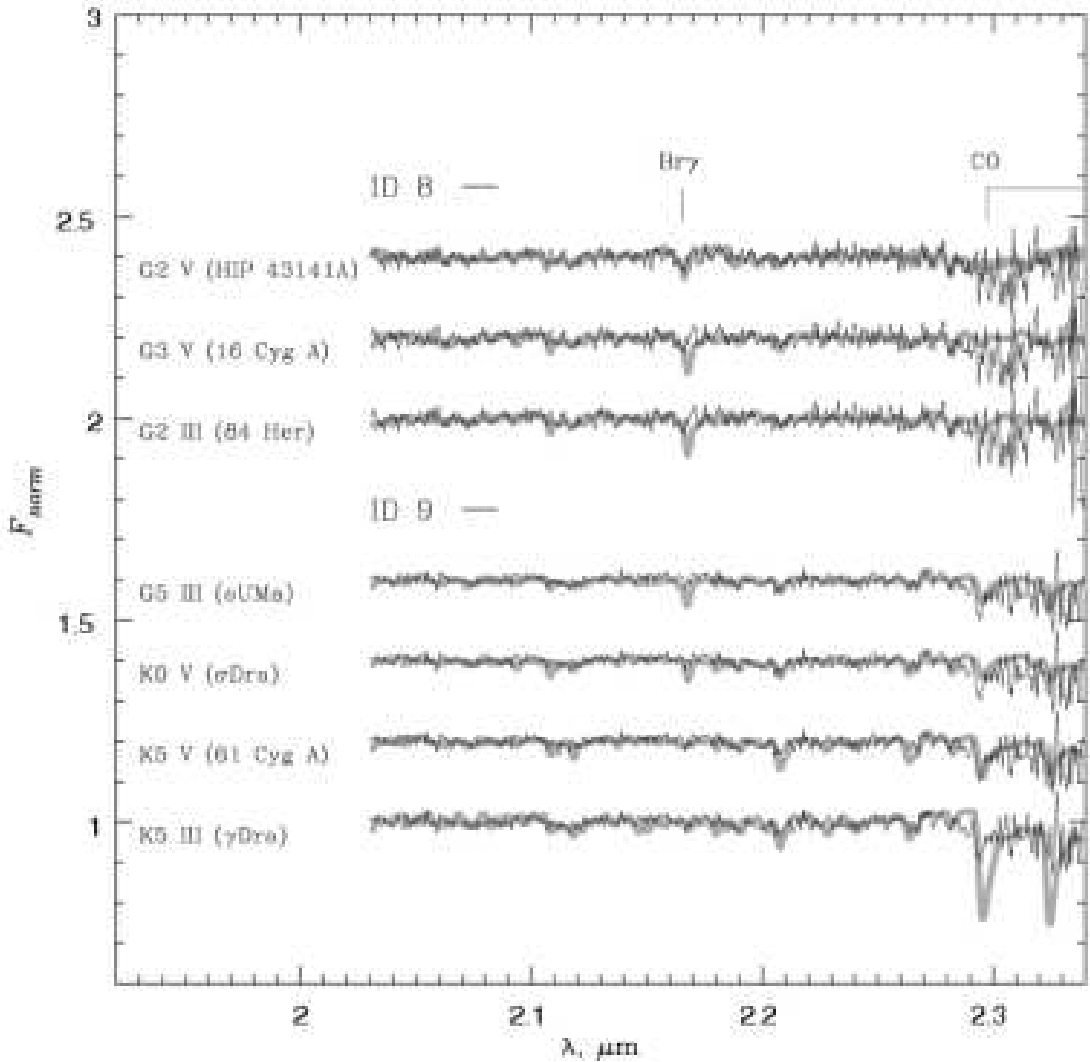


FIG. 13.— SofI spectra of ID 8 & 9 (*thin black lines*) compared to the spectra of standard stars from Kleinmann et al. (1986), and to HIP 43141A obtained on the same night (*thick gray lines*). Standard spectra have been smoothed to match the SofI resolution. All spectra have been continuum normalized and shifted in the vertical direction (except  $\gamma$  Dra). The spectrum of ID 8 is consistent with a G type, while the spectrum of ID 9 matches a mid-K dwarf.